# IP6K1 upregulates the formation of processing bodies by influencing protein-protein interactions on the mRNA cap

Akruti Shah[1,2] and Rashna Bhandari[1*]

[1]Laboratory of Cell Signalling, Centre for DNA Fingerprinting and Diagnostics (CDFD), Inner Ring Road, Uppal, Hyderabad 500039, India.
[2]Graduate studies, Manipal Academy of Higher Education, Manipal 576104, India.

*Correspondence to Rashna Bhandari; **Email:** rashna@cdfd.org.in

**ORCID IDs**

Akruti Shah - 0000-0001-9557-4952
Rashna Bhandari - 0000-0003-3101-0204

**Preprint –** A version of this manuscript has been posted on the preprint server bioRxiv
doi: https://doi.org/10.1101/2020.07.13.199828

**Keywords:** mRNA decay / mRNA metabolism / P-bodies / DDX6

**List of symbols and abbreviations used:**

ATP - adenosine triphosphate; BSA - bovine serum albumin; CHX – cycloheximide; DAPI - 4’6-diamidino-2-phenylindole; DMEM - Dulbecco’s modified Eagle’s medium; DTT – dithiothreitol; FBS - fetal bovine serum; HEPES - 4-(2-hydroxyethyl)-1-piperazineethanesulfonic acid; IP6 - inositol hexakisphosphate; IP7 - diphosphoinositol pentakisphosphate; $m^7$GTP - 7-Methyl-guanosine-5'-triphosphate; P-bodies - processing bodies; PBS - phosphate buffered saline; RT-qPCR - quantitative reverse transcription PCR; s.e.m. - standard error of the mean

**Summary statement**

Inositol hexakisphosphate kinase 1, independent of its enzyme activity, engages in protein-protein interactions on the mRNA cap to promote translational suppression and upregulate the formation of processing bodies.

**Abstract**

Inositol hexakisphosphate kinase 1 (IP6K1) is a small molecule kinase that catalyzes the conversion of the inositol phosphate IP6 to 5-IP7. We show that IP6K1 acts independent of its catalytic activity to upregulate the formation of processing bodies (P-bodies), which are cytoplasmic ribonucleoprotein granules that store translationally repressed mRNA. IP6K1 does not localize to P-bodies, but instead binds to ribosomes, where it interacts with the mRNA decapping complex - the scaffold protein EDC4, activator proteins DCP1A/B, decapping enzyme DCP2, and RNA helicase DDX6. Along with its partner 4E-T, DDX6 is known to nucleate protein-protein interactions on the 5' mRNA cap to facilitate P-body formation. IP6K1 binds the translation initiation complex eIF4F on the mRNA cap, augmenting the interaction of DDX6 with 4E-T and the cap binding protein eIF4E. Cells with reduced IP6K1 show downregulated microRNA-mediated translational suppression and increased stability of DCP2-regulated transcripts. Our findings unveil IP6K1 as a novel facilitator of proteome remodelling on the mRNA cap, tipping the balance in favour of translational repression over initiation, thus leading to P-body assembly.

**Introduction**

Inositol hexakisphosphate kinases (IP6Ks) catalyse the synthesis of the small signalling molecule 5-diphosphoinositol pentakisphosphate (5PP-IP5 or 5-IP7) from inositol hexakisphosphate (IP6) (Saiardi et al., 1999; Thomas and Potter, 2014). Mammals have three isoforms of IP6Ks – IP6K1, IP6K2, and IP6K3, which exhibit similarities in their C-terminal domains and divergence at their N-termini (Saiardi et al., 1999; Saiardi et al., 2001; Wang et al., 2014). IP6Ks have been shown to influence a variety of cellular and physiological processes in mammals, by virtue of their ability to synthesize 5-IP7, and also via protein-protein interactions that are independent of their catalytic activity (Thomas and Potter, 2014). The loss of IP6K1 in mice results in male-specific infertility, primarily due to incomplete sperm maturation (Bhandari et al., 2008). We have shown that IP6K1 is expressed at high levels in round spermatids, where it is essential for the formation of perinuclear ribonucleoprotein (RNP) granules called chromatoid bodies (Malla and Bhandari, 2017). The absence of chromatoid bodies in *Ip6k1* knockout mice leads to premature translation of key spermiogenic proteins, resulting in defects in spermiogenesis, and concomitant infertility (Malla and Bhandari, 2017). The functional analogue of chromatoid bodies in somatic cells are called processing bodies or P-bodies (Kotaja et al., 2006). These cytoplasmic RNP

granules are thought to primarily be sites for mRNA storage (Standart and Weil, 2018; Zhang and Herman, 2020), and harbour proteins involved in suppression of mRNA translation (Ferraiuolo et al., 2005; Kamenska et al., 2016; Liu et al., 2005). P-bodies are also enriched in proteins that participate in 5'-3' mRNA degradation, including proteins responsible for mRNA deadenylation, mRNA decapping, and 5'-3' exoribonuclease activity (Cougot et al., 2004; Luo et al., 2018; Parker and Sheth, 2007; Sheth and Parker, 2003; Zheng et al., 2008).

Proteins involved in suppression of mRNA translation are essential for the *de novo* formation of P-bodies (Ayache et al., 2015). mRNA translation and mRNA decay are intimately linked - both processes require the mutually exclusive binding of multiprotein complexes to the $m^7$GTP mRNA cap. The translation initiation factor eIF4E, and the mRNA decapping enzyme DCP2, compete to bind the mRNA cap (Ramirez et al., 2002; Schwartz and Parker, 2000; Vilela et al., 2000). A proteome exchange at the mRNA cap, where the decapping complex replaces the translation initiation complex, is pre-requisite for P-body formation. Translational suppressors, including the RNA helicase DDX6 and the eIF4E binding protein 4E-T, mediate multivalent interactions that facilitate this proteome switch (Arribas-Layton et al., 2013; Ferraiuolo et al., 2005; Haas et al., 2010; Hubstenberger et al., 2017). However, less is known about the factors that assist or regulate DDX6/4E-T-mediated mRNP remodelling during the transition from translation to suppression,

Here, we introduce IP6K1 as a novel factor that promotes P-body formation. Lowering cellular levels of IP6K1 causes a drastic reduction in the abundance of P-bodies. This effect can be reversed by the expression of active or catalytically inactive IP6K1, but not by IP6K2 or IP6K3, suggesting that a region unique to the IP6K1 isoform engages in protein-protein interactions that upregulate P-body assembly. IP6K1 is distinct amongst several proteins known to facilitate P-body formation, as it regulates events leading to P-body assembly, but does not localize to P-bodies. We uncover multiple IP6K1 interactions that facilitate the DDX6/4E-T-mediated block in translation and downstream mRNA decapping. We show that IP6K1 localises to ribosomes and facilitates proteome exchange on the mRNA cap which is known to enable transition of the transcript from active translation to repression, thus promoting the formation of P-bodies. At the cellular level, we noted that the reduction of P-bodies consequent to a decrease in IP6K1 correlates with reduced miRNA-mediated translational suppression, and increased stability of transcripts that undergo decapping by DCP2.

## Results

### Depletion of IP6K1 disrupts P-body formation

We have previously illustrated that IP6K1 is indispensable for the assembly of chromatoid bodies in round spermatids (Malla and Bhandari, 2017). As chromatoid bodies are similar to P-bodies in terms of their function and composition (Kotaja et al., 2006), we investigated whether IP6K1 depletion also affects the formation of P-bodies. Bronchiolar epithelial sections from either *Ip6k1*$^{+/+}$ or *Ip6k1*$^{-/-}$ mice were subjected to immunostaining to detect the decapping activator protein DCP1A, which is enriched in P-bodies. In sections from *Ip6k1*$^{+/+}$ mice, we observed faint cytoplasmic staining and intense granular staining of DCP1A, indicative of its enrichment in P-bodies (Fig. 1A). However, in *Ip6k1*$^{-/-}$ sections, DCP1A staining was predominantly cytoplasmic, and P-body granules were nearly absent, revealing that IP6K1 is indeed essential for the presence of P-bodies in somatic cells. Next, we examined the human tumour-derived cell lines HeLa and U-2 OS, which normally contain an average of ten P-bodies per cell, and have been used as model systems for the study of P-body assembly and function (Kedersha et al., 2005; Standart and Weil, 2018). We examined HeLa sh*IP6K1* and U-2 OS sh*IP6K1* cell lines, which harbour shRNA directed against *IP6K1* and display a 70-80% knockdown in IP6K1 expression levels compared with control cell lines HeLa shNT and U-2 OS shNT, that express non-targeting shRNA ((Jadav et al., 2013), Fig. S1A). DCP1A immunostaining revealed a drastic reduction in the number of P-bodies in IP6K1 depleted cells compared with non-targeted control cells (Figs. 1B-E). This effect of IP6K1 depletion on P-body abundance was confirmed by the detection of P-bodies using two other marker proteins - the RNA helicase DDX6 and the 5'-3' exoribonuclease XRN1 (Figs. S1B-E). To determine whether IP6K1 is a resident P-body protein, we co-stained U-2 OS cells with antibodies against IP6K1 and DCP1A. As reported earlier (Saiardi et al., 2001), we detected IP6K1 in the nucleus and cytoplasm, but did not observe any co-localization between IP6K1 and DCP1A in P-bodies (Figs. 1F and G). When over-expressed in U-2 OS cells, IP6K1 was enriched in the nucleus, and showed diffuse staining throughout the cell, but was not detected in P-bodies (Fig. S1F). These data indicate that, unlike most proteins involved in P-body assembly, IP6K1 does not localize to P-bodies.

### IP6K1 influences P-body formation independent of its catalytic activity

To determine whether the ability of IP6K1 to synthesize 5-IP7 is essential for the formation of P-bodies, we introduced a single amino acid substitution in human IP6K1, replacing Lys226, which lies within the conserved catalytic sequence PxxxDxKxG, with Ala (Wang et

al., 2014). We confirmed the loss of catalytic activity in this mutant form of IP6K1 (Fig. S2A). Active IP6K1 or kinase-dead IP6K1 (K226A) were introduced into U-2 OS sh*IP6K1* cells. Expression of either version of IP6K1 restored the ability of U-2 OS sh*IP6K1* cells to form P-bodies, indicating that IP6K1 is required for the presence of P-bodies independent of its catalytic activity (Figs. 2A and B; S2B). However, the number of P-bodies per cell was higher in U-2 OS sh*IP6K1* cells expressing active IP6K1 compared with cells expressing the kinase-dead mutant version of IP6K1 (Fig. 2B and S2B). To investigate this further, we overexpressed either active or kinase-dead IP6K1 in native U-2 OS cells. Overexpression of both these versions of IP6K1 caused a significant increase in the number of P-bodies (Figs. 2C and D). However, as noted in the case of U-2 OS sh*IP6K1* cells, the number of P-bodies in native U-2 OS cells overexpressing active IP6K1 was greater than the number of P-bodies seen in cells overexpressing the inactive enzyme (Fig. 2D). We conclude that IP6K1 protein, irrespective of its enzymatic activity, is sufficient for the formation of P-bodies, but that 5-IP7 synthesised by IP6K1 acts to further increase the number of P-bodies per cell. As IP6K2 and IP6K3 share significant sequence similarity with IP6K1, we examined whether IP6K2 or IP6K3 also influence the formation of P-bodies. Overexpression of either IP6K2 or IP6K3 failed to rescue the depletion of P-bodies in U-2 OS sh*IP6K1* cells (Fig. S2C). This data suggests that the ability of IP6K1 to upregulate the formation of P-bodies is dependent on its N-terminal domain, which shows greater sequence divergence between the three IP6K paralogs (Saiardi et al., 1999; Saiardi et al., 2001; Wang et al., 2014). Next, we tested whether a chemical stressor known to increase P-body abundance can counter the effect of IP6K1 depletion on P-bodies. Vinblastine, an inhibitor of microtubule assembly, has been shown to induce P-bodies in U-2 OS cells (Aizer et al., 2008; Ayache et al., 2015). We treated U-2 OS shNT and U-2 OS sh*IP6K1* cells with vinblastine, and confirmed microtubule disassembly by staining cells to detect α-tubulin aggregates (Fig. S3). We observed an increased abundance of P-bodies in both cell types compared with vehicle-treated control cells (Fig. S3B). More importantly, there was no difference in the number of P-bodies between vinblastine treated U-2 OS shNT and U-2 OS sh*IP6K1* cells, whereas, as expected, IP6K1 downregulation reduced P-body abundance in vehicle-treated cells.

**IP6K1 depletion causes down-regulation of key mRNA decapping proteins**

Since IP6K1 does not localise to P-bodies, it may influence P-body formation via indirect regulation of other key P-body components. We therefore investigated whether lowering the expression of IP6K1 affects the level of key P-body resident proteins. We performed

immunoblotting analysis to examine the total cellular levels of components of the mRNA decapping complex, including the scaffold protein EDC4, the decapping enzyme DCP2, and the decapping activator proteins DCP1A and DCP1B. Interestingly, knocking down IP6K1 expression by 70% in U-2 OS sh*IP6K1* cells resulted in a 40-70% reduction in the levels of EDC4, DCP1A/B, and DCP2, when compared with U-2 OS shNT cells (Figs. 3A and B). However, this reduction in the level of decapping proteins in U-2 OS sh*IP6K1* cells is independent of any change in the abundance of their mRNA transcripts (Fig. S4A). We were able to restore EDC4 and DCP1A expression in U-2 OS sh*IP6K1* by over-expressing either active or inactive IP6K1, suggesting that IP6K1 maintains the levels of decapping proteins independent of its catalytic activity (Figs. S4B and C). We also examined the expression level of other P-body marker proteins including the RNA helicase DDX6, which suppresses mRNA translation, PAN3, which deadenylates mRNA prior to decapping, the 5'-3' exoribonuclease XRN1, which degrades decapped mRNA, and GW182, a scaffolding protein involved in micro-RNA mediated mRNA degradation. Unlike the decapping protein complex, knocking down IP6K1 expression did not lower the cellular levels of these four proteins that function upstream or downstream to decapping (Figs. 3C and D). As EDC4 downregulation has been shown to lower DCP2 levels and reduce the number of P-bodies (Chang et al., 2014; Erickson et al., 2015; Yu et al., 2005), we attempted to rescue the depletion of P-bodies in U-2 OS sh*IP6K1* cells by overexpressing EDC4. Immunostaining to detect DCP1A revealed that EDC4 overexpression does indeed restore P-body formation, when compared with untransfected cells in the same sample (Figs. 3E and F).

We next examined whether overexpression of IP6K1, which increases the abundance of P-bodies (Figs. 2C and D), is accompanied by an increase in the expression of mRNA decapping proteins. The levels of EDC4, DCP1A and DCP2 however remained unaltered upon overexpression of either active or inactive IP6K1 (Figs. S4D and E). This data indicates that IP6K1 does not regulate P-body formation merely by controlling the expression level of mRNA decapping proteins, and points to an additional layer of regulation of P-body formation by IP6K1.

**IP6K1 interacts with the mRNA decapping complex on ribosomes**

To further explore the mechanism by which IP6K1 influences P-body dynamics, we sought to check if IP6K1 binds any of the mRNA decapping proteins. For this we turned to HEK293T cells, which possess a high efficiency of transfection, where we first confirmed that IP6K1

overexpression does indeed increase the abundance of P-bodies (Fig. S5A). IP6K1, tagged with either SFB or V5 epitopes, was able to pull down endogenous DCP1A, DCP2 and EDC4 in HEK293T cells (Figs. 4A and B, S5B). IP6K1 also interacted with the RNA helicase DDX6 (Fig. 4C), another component of the mRNA decapping complex, which is known to promote P-body assembly by repressing translation initiation (Ayache et al., 2015). However, the mRNA deadenylase PAN3, also a component of P-bodies, did not bind IP6K1 (Fig. 4A), supporting the specificity of the interaction of IP6K1 with the mRNA decapping complex. The other two IP6K paralogs, IP6K2 and IP6K3, which do not promote the formation of P-bodies (Fig. S2C), were unable to pull down DCP1A or EDC4 (Fig. S5C and D), further supporting the specificity of the interaction between IP6K1 and these proteins. We raised an antibody directed against the N-terminus of IP6K1 and validated its specificity (Fig. S5E and S5F). This antibody was used to pull down endogenous IP6K1 from HEK293T cells (Fig. 4D and S5G). The decapping complex proteins DCP1A and DDX6 co-immunoprecipitated with IP6K1 (Fig. 4D), but we did not observe binding of the decapping enzyme DCP2 to endogenous IP6K1 (Fig. S5G). For EDC4, we detected multiple bands co-precipitating with IP6K1 (Fig. S5G), and were therefore unable to confirm the binding of EDC4 to endogenous IP6K1. The interaction of endogenous IP6K1 with DCP1A and DDX6 persisted even after RNase A treatment of cell lysates, indicating that the binding of IP6K1 to the mRNA decapping complex is RNA-independent (Fig. S5H). To determine whether the interaction between IP6K1 and proteins of the decapping complex is direct or indirect, we immobilized bacterially-expressed GST-tagged DDX6, DCP1A, or DCP2 and incubated them with purified hexahistidine-tagged IP6K1. We observed a direct interaction of DDX6 and DCP2 with IP6K1 (Fig. S5I). As DCP1A tagged with GST was highly susceptible to degradation (Fig. S5I), and EDC4 protein is not amenable for expression in bacteria due to its large size, we could not interrogate the direct binding of these proteins with IP6K1. Our protein-protein interaction data thus reveals that IP6K1 interacts directly with at least two components of the decapping complex – DCP2 and DDX6.

Our data show that IP6K1 specifically interacts with P-body-enriched mRNA decapping proteins, but that IP6K1 is itself not localized to P-bodies. Therefore, this protein-protein interaction is likely to occur at another sub-cellular compartment. In budding yeast, plants, and mammals, several proteins involved in mRNA decapping and degradation have been shown to localize to ribosomes, and facilitate co-translational degradation of stalled mRNAs (Pelechano et al., 2015; Sweet et al., 2012; Wang et al., 2002; Weidner et al., 2014). To

examine the possibility that IP6K1 interacts with the mRNA decapping machinery on ribosomes, we first checked if IP6K1 localizes to ribosomes in mammalian cells. We fractionated U-2 OS and HEK293T cell extracts, and obtained a pure ribosomal fraction, as evidenced by the absence of the cytoplasmic marker GAPDH, and enrichment of small and large ribosomal subunit proteins RPS6 and RPL6 respectively (Fig. 4E and S5J). We detected the presence of IP6K1 along with the mRNA decapping complex (DCP1A, DCP2, and EDC4) in the ribosomal fraction obtained from U-2 OS and HEK293T cells (Fig. 4E and S5J). To determine whether the interaction between IP6K1 and mRNA decapping proteins occurs on ribosomes, we purified the ribosomal fraction from HEK293T cells expressing tagged IP6K1. Co-precipitation of the ribosomal marker RPS6 with IP6K1 confirmed that IP6K1 is indeed present in ribosomes (Fig. 4F). The endogenous decapping complex proteins DCP1A, DCP2, EDC4 and DDX6 were also pulled down with IP6K1 from the ribosomal fraction (Fig. 4F and G). The mRNA deadenylase PAN3 was present in the ribosomal fraction but did not co-precipitate with IP6K1, and thus served as a negative control.

**IP6K1 facilitates the interaction between the translation initiation factor eIF4E and translational suppressors 4E-T/DDX6 on the mRNA cap**

An early event in the formation of P-bodies is the exchange of proteins bound to translationally stalled mRNA – proteins responsible for active translation are replaced with proteins involved in mRNA degradation. We hypothesized that the presence of IP6K1 on ribosomes may facilitate this proteome switch. Since IP6K1 interacts with the mRNA decapping complex, we examined whether it also binds to the translation initiation complex eIF4F. A pull-down of Myc epitope-tagged IP6K1 revealed specific interaction with all three members of the eIF4F translation initiation complex - the cap binding protein eIF4E, the RNA helicase eIF4A2, and the scaffolding protein eIF4G1 (Fig. 5A and B). The N-terminally directed IP6K1 antibody was able to co-precipitate eIF4G1 with endogenous IP6K1, but eIF4A2 and eIF4E were not detectable in this pull-down (Fig. 5C). We were however able to detect a direct interaction between bacterially-expressed GST-tagged eIF4E and hexahistidine-tagged IP6K1, suggesting that IP6K1 does indeed interact directly with eIF4E (Fig. S6A). A similar direct interaction was not observed between eIF4A2 and IP6K1 (Fig. S6A). As eIF4G1 is too large for heterologous expression in bacteria, it is unclear whether the interaction between IP6K1 and eIF4G1 is direct or indirect.

In translationally stalled mRNA, eIF4E bound to the $m^7$GTP cap is replaced with the decapping enzyme DCP2 (Schwartz and Parker, 2000). To determine if IP6K1 facilitates this exchange, we first examined whether endogenous IP6K1 interacts with eIF4E on the mRNA cap. Incubation of U-2 OS cell extract with immobilised $m^7$GTP cap analogue revealed that IP6K1 is bound to the mRNA cap, along with eIF4E (Fig. 5D). To ensure that this pull-down is specific, we treated the cell lysate with monomethylated cap analogue ($m^7$GpppG), to competitively deplete eIF4E bound to $m^7$GTP beads. The amount of both eIF4E and IP6K1 bound to $m^7$GTP beads was reduced in the presence of $m^7$GpppG, indicating that IP6K1 is specifically recruited to the mRNA cap (Fig. 5D). We confirmed that the interaction between IP6K1 and eIF4E on the mRNA cap is RNA-independent by demonstrating that treatment with RNase A prior to the pull-down does not alter the extent of interaction of IP6K1 or eIF4E with the $m^7$GTP beads (Fig. S6B).

The eIF4E transporter protein 4E-T, supresses cap-dependent translation upon binding to eIF4E, and is indispensable for the formation of P-bodies (Ferraiuolo et al., 2005). To investigate if IP6K1 regulates 4E-T binding to eIF4E, we pulled down eIF4E from U-2 OS shNT and sh*IP6K1* cells using immobilised $m^7$GTP cap analogue. We observed a significant reduction in the interaction of 4E-T with eIF4E in cells with lower levels of IP6K1, although the expression of 4E-T protein remains unaltered (Figs. 5E and G). The level of expression of eIF4E, eIF4G1, and eIF4A2, or their binding to the mRNA cap analogue, was not affected by a reduction in IP6K1 (Fig. 5E-G). 4E-T is known to interact with the RNA helicase DDX6 (Ayache et al., 2015; Kamenska et al., 2016), and this interaction is required for micro-RNA dependent suppression of translation and for the formation of P-bodies. We noted that the $m^7$GTP cap analogue pulls down DDX6 from a U-2 OS cell extract, indicating that DDX6 and 4E-T are both bound to eIF4E (Fig. 5F). The binding of DDX6 to the $m^7$GTP cap analogue was significantly reduced in cells expressing lower levels of IP6K1 (Fig. 5F and G). These data suggest that IP6K1 promotes the binding of the DDX6/4E-T complex to eIF4E on the mRNA cap. To further examine this possibility, DDX6 fused with GFP was immunoprecipitated in the presence or absence of overexpressed IP6K1 in HEK293T cells. The expression of active or catalytically inactive IP6K1 led to a significant increase in the binding of both eIF4E and 4E-T to DDX6 (Fig. 5H and I). Thus, independent of its catalytic activity, IP6K1 promotes the interaction of translational suppressors essential for P-body formation with the translation initiation factor eIF4E. DDX6 is known to have multivalent interactions with translational suppressors and with mRNA decapping proteins (Ayache et al.,

2015). To determine whether IP6K1 also regulates the binding of the mRNA decapping complex to DDX6, we examined the co-immunoprecipitation of EDC4 with DDX6. There was a notable increase in the level of endogenous EDC4 interacting with GFP-DDX6 upon the overexpression of either active or catalytically inactive IP6K1 (Fig. 5J and K).

**Functional consequences of IP6K1 depletion on mRNA metabolism**

The interaction between DDX6 and 4E-T has been shown to be important for microRNA (miRNA)-mediated suppression of translation, and the subsequent formation of P-bodies (Kamenska et al., 2016). As IP6K1 promotes the binding of 4E-T to DDX6 (Fig. 5H and I), we investigated whether a decrease in cellular IP6K1 levels affects miRNA-mediated mRNA suppression. We employed a miRNA reporter assay that utilizes a Renilla luciferase (RL) coding sequence with a let7a miRNA binding site in the 3'UTR, which is either a site for perfect complementary binding (pRL-perf) or binding with three sets of mismatches (pRL-3XB) (Fig. 6A). When bound to let7a miRNA, the RL-perf reporter mRNA is cleaved endonucleolytically, but the RL-3XB mRNA is translationally stalled (Pillai et al., 2005). Any decrease in let7a miRNA mediated mRNA cleavage or translational suppression, is recorded as an increase in RL activity. We noted no change in RL activity encoded by the pRL-perf reporter in HeLa sh*IP6K1* cells compared with HeLa shNT cells, implying that IP6K1 has no effect on endonucleolytic cleavage of the reporter mRNA (Fig. 6A). However, RL expression by the pRL-3XB reporter was significantly higher in HeLa sh*IP6K1* cells compared with HeLa shNT cells, indicating that IP6K1 promotes miRNA-mediated translational suppression. We did not observe any significant difference in the polysome profiles or the polysome-to-monosome ratios between the two cell types, indicating that the loss of IP6K1 has no effect on global translation (Fig 6B).

As IP6K1 overexpression leads to increased binding of the mRNA decapping complex scaffold protein EDC4 to DDX6 (Fig. 5 J and K), we examined whether this strengthened interaction leads to an increase in mRNA decapping. We co-overexpressed GFP-tagged decapping enzyme DCP2 with IP6K1 in HEK293T cells. Immunoprecipitated GFP-DCP2 was incubated with radiolabelled $m^7$GTP-capped mRNA, the products were resolved by thin layer chromatography, and the magnitude of decapping was monitored by densitometry analysis of the decapping product $m^7$GDP. We observed an approximately 40% increase in the extent of decapping when GFP-DCP2 was co-expressed with IP6K1 as compared with the vector control (Fig. 6C and D). As expected, co-expression of IP6K2, which does not

promote P-body assembly, did not increase the activity of the mRNA decapping complex. We confirmed that the presence of either IP6 kinase did not alter the level of expression or immunoprecipitation of GFP-DCP2 compared with the vector control (Fig. 6E). As IP6K1 upregulates DCP2-mediated mRNA decapping, we expect that depletion of IP6K1 would lead to stabilization of mRNA that are known to be decapped by DCP2 (Luo et al., 2020). We monitored mRNA stability by comparing the levels of specific transcripts in the presence versus absence of the transcription inhibitor Actinomycin D. In U-2 OS cells expressing non-targeting shRNA, 18 out of the 24 tested DCP2 substrate mRNAs showed a significant decline in cells treated with Actinomycin D compared with untreated cells, which is indicative of the degradation of these transcripts (Fig. 6F). However, 17 out of these 18 transcripts did not show any significant decline in their levels in U-2 OS sh*IP6K1* cells. To confirm that the increase in mRNA stability in U-2 OS sh*IP6K1* compared with U-2 OS shNT cells reflects a difference in mRNA half-life, we monitored the levels of selected mRNA in both cell types over a time course following Actinomycin D treatment. We were able to determine the half-life of five different mRNA expressed in U-2 OS shNT cells, whereas the same mRNA expressed in U-2 OS sh*IP6K1* cells showed either an increase in half-life, or no degradation during the time course of the experiment (Fig. S6C). These data clearly reveal that the loss of IP6K1 leads to stabilization of DCP2-targeted transcripts, and provides a functional readout for the role of IP6K1 in promoting DCP2-mediated decapping.

**Discussion**

Our work reveals that IP6K1 is a key player in the regulation of mRNA turnover and P-body formation. Unlike its involvement in the assembly of chromatoid bodies as an integral component, IP6K1 promotes P-body formation without actually localizing to P-bodies. It does this primarily by facilitating translational repression of mRNAs that are destined for P-bodies (Fig. 7). IP6K1 is bound to ribosomes, where it interacts with the mRNA decapping machinery, including EDC4, DCP1A, and DCP2, and the RNA helicase DDX6. We also show that IP6K1 binds the eIF4F translation initiation complex (eIF4G1, eIF4E and eIF4A), and promotes the interaction of DDX6 and 4E-T with the cap binding protein eIF4E. The interaction between DDX6 and 4E-T, and the binding of 4E-T to eIF4E, have been shown to enhance the miRNA-mediated suppression of translation (Kamenska et al., 2016). Our data therefore suggests that IP6K1 facilitates proteome remodelling on the mRNA cap, to tip the scales in favour of DDX6/4E-T-mediated translational repression over translation initiation, and feed P-body formation (Fig. 7).

Our work shows that the influence of IP6K1 on the formation of P-bodies is largely independent of its catalytic activity. Overexpression of either active or inactive forms of IP6K1 can induce the formation of P-bodies in U-2 OS cells (Fig. 2 and S2B). However, we do observe a statistically significant difference in the number of P-bodies that accumulate upon over-expression of these two forms of IP6K1, with the catalytically inactive form of IP6K1 inducing fewer P-bodies compared with the active form (Figs. 2B and D, S2B). This data is in concurrence with the recent demonstration by Shears and colleagues that an increase in intracellular levels of 5-IP7 upregulates the formation of P-bodies (Sahu et al., 2020). The Shears laboratory reports that 5-IP7 competes with the $m^7$GTP mRNA cap for binding to NUDT3, a diphosphoinositol polyphosphate phosphohydrolase, which is known to decap a subset of mRNAs independent of DCP2. In cells with increased 5-IP7, there is an accumulation of NUDT3 mRNA substrates, and a consequent elevation in the abundance of P-bodies. IP6K1 thus influences the formation of P-bodies via two different mechanisms – by 5-IP7-dependent inhibition of NUDT3-mediated mRNA decapping, and by enzymatic activity independent facilitation of protein-protein interactions that promote DCP2-dependent mRNA decapping.

Our study also shows that a decrease in IP6K1 leads to a reduction in the levels of mRNA decapping proteins EDC4, DCP1A/B and DCP2 (Figs. 3A and B). The mechanism by which IP6K1 regulates the levels of mRNA decapping proteins remains unclear. It is possible that the decrease in translational suppression in cells expressing sh*IP6K1* has a cascading effect on the stability of decapping proteins. Alternatively, IP6K1 may indirectly regulate the levels of decapping proteins by influencing their expression or stability, independent of the effect of IP6K1 on translational suppression. Nonetheless, a reduction in the level of the decapping scaffold protein EDC4, which is essential for P-body formation, combined with reduced DDX6/4E-T-mediated translational suppression, results in a decrease in P-bodies in cells depleted for IP6K1.

In conclusion, our study demonstrates that the small molecule kinase IP6K1 acts independent of its enzymatic activity to moonlight as a regulator of mRNA metabolism. IP6K1 engages in an array of interactions with multiple RNA binding protein complexes, and influences several protein-protein interactions to promote P-body assembly.

## Materials and Methods

**Reagents:** All chemicals were procured from Sigma-Aldrich, unless specified otherwise. The primary antibodies used in this study for immunofluorescence (IF), immunoblotting (IB) or immunoprecipitation (IP), along with antibody dilution for each application, and supplier (including catalogue number) are as follows: anti-IP6K1 (Sigma-Aldrich, HPA040825; IF 1:500; IB 1:2000), anti-GAPDH (Sigma-Aldrich, G8795; IB 1:10,000), anti-α-tubulin (Sigma-Aldrich, T9026; IB 1:10,000, IF 1:800), anti-V5 tag (Thermo Fisher Scientific, R960-25; IB 1:5000, IP 1µg, and Abcam, Ab53418; IF 1:800), anti-GFP (Invitrogen, A11122; IB 1:5000, IP 2 µg), anti-HA (Sigma-Aldrich, H6908; IF: 1:500); anti-FLAG (Sigma-Aldrich, F1804; IB 1:10,000, IP 1 µg); anti-myc (Sigma-Aldrich, M4439; IB 1:10,000, IP 1 µg; IF: 1:800); anti-DCP1A (Abcam, Ab47811, Ab57654; IF 1:400, IB 1:200); anti-DCP1B (Abcam, Ab222313; IB 1:1000); anti-DCP2 (Sigma-Aldrich, D6319; IB 1:2000); anti-EDC4 (Abcam, Ab72408; IB 1:2000); anti-PAN3 (Abcam, Ab189413; IB 1:2000); anti-GW182 (Abcam, Ab156173; IB 1:1000); anti-DDX6 (Novus Biologicals, NB200-191; IF 1:400, IB 1:2000); anti-XRN1 (Abcam, Ab70259; IB 1:2000; IF 1:400); anti-eIF4G1 (Cell Signaling Technology, 8701S; IB 1:2000); anti-eIF4E (Novus Biologicals, MAB3228; IB 1:1000); anti-eIF4A2 (Novus Biologicals, NBP2-24529; IB 1:1000); anti-4E-T (Invitrogen, A300706AT; IB 1:2000); anti-RPS6 (Cell Signaling Technology, 2217S; IB 1:5000); anti-RPL6 (GeneTex, GTX114913; IB:1:5000); anti-6xHis tag (Abcam, Ab18184; IB 1:10,000). Restriction enzymes were purchased from New England Biolabs. The dual luciferase reporter assay kit was purchased from Promega (E1910). Dulbecco's Modified Eagle Medium (DMEM), Fetal Bovine Serum (FBS) and other cell culture reagents were from Thermo Fisher Scientific. $m^7$GTP cap analogue beads (AC-155S), $m^7$GTP (NU-1122S), $m^7$GDP (NU-1134S), $m^7$GMP (NU-1135S), and $m^7$GpppG cap analogue (NU-852S) were purchased from Jena Bioscience. NuPAGE 4-12% Bis-Tris gels were from Thermo Fisher Scientific. [α-$^{32}$P]GTP was procured from JONAKI/BRIT. The in vitro transcription and mRNA capping kit was purchased from CellScript (C-MSC11610).

**Plasmids:** Human IP6K1 cDNA (GenBank ID NM_001242829.2) was sub-cloned into the NheI and BamHI restriction enzyme sites in the pCDNA 3.1 cMYC-V5 expression plasmid (Lolla et al., 2021), such that cMYC was replaced by IP6K1 to obtain a C-terminally V5 epitope-tagged IP6K1 plasmid. A catalytically inactive version of human IP6K1 was prepared by using this plasmid to substitute Lys226 with Ala by site-directed mutagenesis and overlap extension PCR, and confirmed by DNA sequencing. Mouse IP6K1 was sub-

cloned into SFB (S-protein/FLAG/SBP) - tagged destination vector using the Gateway cloning strategy (Invitrogen). Catalytically inactive IP6K1 (K226A) was generated by site-directed mutagenesis and overlap extension PCR, and cloned into SFB-tagged destination vector. For expression as GST fusion proteins in *E. coli*, full-length human DDX6, DCP2, eIF4E, and eIF4A2 were subcloned into BamHI and XhoI restriction enzyme sites in the plasmid pGEX-6P-2 (GE Life Sciences). Human DCP1A was sub-cloned into GST-tagged destination vector using the Gateway cloning strategy (Invitrogen). Plasmids expressing myc-tagged mouse IP6K1 (GenBank ID NM_013785.2), human IP6K2 (GenBank ID NM_001005909.3) and human IP6K3 (GenBank ID NM_001142883.2) were gifts from Solomon Snyder (Johns Hopkins School of Medicine, Baltimore, USA). pT7-EGFP-C1-HsRCK (DDX6) (Addgene plasmid # 25033; GenBank ID NM_004397), pCIneo-lambdaN-HA-HsEDC4 (Addgene plasmid # 66597; GenBank ID NM_014329.4) and pT7-EGFP-C1-HsDCP2 (Addgene plasmid # 25031; GenBank ID AY146650) were gifts from Elisa Izaurralde (Max Planck Institute for Developmental Biology, Tübingen, Germany).

**Cell lines and transfection:** All cell lines were grown in a humidified incubator with 5% $CO_2$ at 37°C in Dulbecco's Modified Eagle Medium (DMEM) supplemented with 10% fetal bovine serum, 1 mM L-glutamine, 100 U/mL penicillin, and 100 µg/mL streptomycin. The cell lines used in this study have been authenticated and tested for contamination. HeLa shNT and sh*IP6K1* cell lines, generated using non-targeting shRNA (SHC016, Sigma-Aldrich) and shRNA directed against human IP6K1 (TRC0000196808, Sigma-Aldrich) respectively, have been described earlier (Jadav et al., 2016). U-2 OS shNT and sh*IP6K1* cell lines were generated similarly, except that a different IP6K1-targeting shRNA was used. Briefly, lentiviral vectors (pLKO.1) encoding either the non-targeting shRNA or shRNA directed against human *IP6K1* (TRC0000013508, Sigma-Aldrich) were co-transfected with VSV-G and psPAX2 (a gift from Didier Trono, Swiss Federal Institute of Technology, Lausanne, Switzerland; Addgene plasmid #12260) plasmids into the HEK293T packaging cell line, using polyfectamine reagent (Qiagen), and incubated at 37°C to generate lentiviral particles. After 48 h, the culture supernatant was passed through a 0.45 µm filter to harvest viral particles, and infect U-2 OS cells following treatment with polybrene (8 µg/mL, Sigma-Aldrich) for 2 h. 2 µg/mL puromycin (Sigma-Aldrich) was added to cells after 48 h to select transduced cells. The extent of knockdown was determined by immunoblot analysis with an IP6K1 specific antibody. For transfection, polyethylenimine (PEI) (Polysciences, 23966) was used at a ratio of 1:3 (DNA:PEI). All plasmids used for transfection were purified using the

Plasmid Midi kit (Qiagen). Cells were harvested 36-48 h post-transfection for further analyses.

**Mice:** All animal experiments were approved by the Institutional Animal Ethics Committee (Protocol number EAF/CDFD/RB/01), and were performed in compliance with guidelines provided by the Committee for the Purpose of Control and Supervision of Experiments on Animals, Government of India. *Ip6k1*$^{+/+}$ and *Ip6k1*$^{-/-}$ mice *(Mus musculus*, strain C57BL/6) used for this study were housed in the Experimental Animal Facility at the Centre for DNA Fingerprinting and Diagnostics, Hyderabad. *Ip6k1*$^{+/+}$ and *Ip6k1*$^{-/-}$ littermates were produced by breeding *Ip6k1*$^{+/-}$ mice and maintained as previously described (Bhandari et al., 2008). The experiments performed in this study did not require mice to be anaesthetized. Lung tissue was isolated from 3-5 month old *Ip6k1*$^{+/+}$ and *Ip6k1*$^{-/-}$ male mice after euthanizing them by CO2 asphyxiation.

**Immunofluorescence analysis:** Cells grown on glass coverslips placed in a 24 well plate were fixed with 4% formaldehyde for 10 min at room temperature (RT), and permeabilized with 0.15% Triton-X 100 for 10 min at RT. Non-specific antibody binding was blocked by incubating the cells in a blocking buffer (3% BSA in PBS with 0.1% Triton-X 100) for 1 h at RT. After blocking, primary antibody diluted in the blocking buffer was added to the cells, and incubated overnight at 4°C. Cells were washed with PBS three times, incubated with fluorophore conjugated secondary antibodies (Alexa Fluor 488 or Alexa Fluor 568 goat anti-rabbit or anti-mouse IgG; 1:500) diluted in the blocking buffer, and incubated for 1 h at RT. Cells were washed with PBS three times, and the coverslips were mounted on glass slides using an antifade mounting medium with DAPI (H-1200, Vecta Labs), air dried and sealed. Where indicated, the cells were treated with 10 µM vinblastine for 1 h prior to fixation, and processed as detailed above. For P-body staining of bronchiolar epithelium tissue, paraffin embedded sections of lung tissue from *Ip6k1*$^{+/+}$ and *Ip6k1*$^{-/-}$ mice were treated with xylene for deparaffinization, dipped in a series of graded ethanol for dehydration, and boiled in 10 mM sodium citrate buffer, pH 6, for 10 min to achieve antigen retrieval. The sections were then washed, permeabilized, and stained as detailed above. Images were acquired on a Zeiss LSM 700 confocal microscope equipped with 405, 488 and 555 nm lasers, and fitted with a 63x, 1.4 NA objective. The exposure settings and other imaging parameters were identical for images of different cell types / treatment conditions in a single experiment. All images are z-stacks showing xy, yz and xz dimensions as a maximum intensity projection (MIP). The

number of P-bodies per cell was quantified using Fiji software (Schindelin et al., 2012), as described earlier (Maquat and Kiledjian, 2008). Briefly, z-stacks (step size 0.5 µm) were digitally collapsed, and the threshold for P-body quantification was set using Otsu thresholding plugin. P-bodies were counted using the 'analyse particles' feature of Fiji, where pixel range to be counted as P-bodies was set at 7 - 500.

**IP6 kinase enzyme activity assay:** IP6K1-V5 or IP6K1-V5 K226A were expressed in HEK 293T cells, immunoprecipitated with anti-V5 antibody and immobilised on Protein A beads. The beads were incubated with 200 µM $IP_6$, 50 µM $Mg^{2+}$-ATP, and 3 µCi [$\gamma$-$^{32}$P]ATP in assay buffer [20 mM HEPES pH 6.8, 6 mM $MgSO_4$, 50 mM NaCl, and 2 mM DTT], for 1 h at 37°C. The reaction was terminated by the addition of 3 mM EDTA, and deproteinized in the presence of 0.6 M $HClO_4$. The sample was neutralized by the addition of 0.3 M $K_2CO_3$ and 5 mM EDTA, and the precipitated protein along with excess $KClO_4$ was removed by centrifugation at 10,000 *g* for 5 min at 25°C. The supernatant was resolved by SAX-HPLC as described in (Jadav et al., 2016). 1 mL fractions were counted with 3 mL scintillation cocktail (Ultima-Flo AP, Perkin Elmer) in a scintillation counter (PerkinElmer Tri-carb 2900) to identify the 5-$IP_7$ peak.

**Generation of an antibody against the N-terminus of IP6K1:** The commercially available IP6K1-specific antibody that we have used for immunofluorescence and western blotting (Sigma-Aldrich, HPA040825) has been validated by the absence of any signal in tissues derived from *Ip6k1*$^{-/-}$ mice (Malla and Bhandari, 2017). For co-immunoprecipitation of endogenous proteins, to avoid any disruption of protein-protein interaction by the antibody, we generated an IP6K1-specific antibody to a unique sequence located at the extreme N-terminus of IP6K1. cDNA encoding the N-terminal 22 amino acid residues (aa) of mouse IP6K1 (NCBI CCDS ID: CCDS23514.1), which is identical in sequence to human IP6K1, was sub-cloned into the BamH I and Xho I restriction enzyme sites in the pGEX-6P-2 expression plasmid. GST-tagged IP6K1 (aa 1-22) was expressed in *Escherichia coli* BL21 (DE3) strain, purified by glutathione affinity chromatography (GE Healthcare, 17-0756-01), dialysed against chilled PBS, and was subsequently used as an antigen to raise rabbit polyclonal antibodies. Generation of the polyclonal antibody was outsourced to Bioklone Biotech Private Limited, Chennai, India. Approval for use of animals for immunisation was provided by the Institutional Animal Ethics Committee (IAEC Approval No. IAEC/I/12 dated 16.09.2017), and was performed in compliance with guidelines provided by the Committee

for the Purpose of Control and Supervision of Experiments on Animals, Government of India. A twelve week old female New Zealand White rabbit was injected subcutaneously with 250 µg of purified antigen emulsified with complete Freund's adjuvant for the first dose, and with 200-250 µg antigen emulsified with incomplete Freund's adjuvant for subsequent booster doses. The animal received 10 booster injections. Sera collected after the terminal booster dose was used for immunoprecipitation. The N-terminus directed IP6K1 antibody was validated by the absence of any immunoprecipitated protein from *Ip6k1*$^{-/-}$ mouse tissues (Fig. S5E), and the specific recognition of IP6K1, but not IP6K2 or IP6K3 (Fig. S5F)

**Co-immunoprecipitation and western blot analysis:** U-2 OS or HEK293T cells were collected after 48 h, and lysed for 1 h at 4˚C in cell lysis buffer (50 mM HEPES pH 7.4, 100 mM NaCl, 1 mM EDTA, 0.5% Nonidet P-40, protease inhibitor cocktail (Sigma P8340), and phosphatase inhibitor cocktail (Sigma P5762)). Specific antibody was added to the lysate and incubated overnight at 4˚C with rotation, and the complex was pulled down using pre-equilibrated Protein A or Protein G Sepharose beads (GE Healthcare) for 1 h. The beads were washed three times with lysis buffer, boiled in 1X Laemmli buffer, and processed using standard western blotting techniques. In all experiments, 3% of the lysate / ribosome fraction was loaded in the input lane, and 90% was used for immunoprecipitation. Chemiluminescence was detected using the UVITEC Alliance Q9 documentation system, or the GE ImageQuant LAS 500 imager. Densitometry analysis of bands was done using Fiji software (Schindelin et al., 2012). In case of HEK293T cells expressing SFB-tagged proteins, pre-equilibrated streptavidin sepharose beads were added to the cell lysate, and incubated for 90 min at 4˚C prior to washing and boiling the beads. In case of RNase experiments, RNase A was added to the lysate at 100 µg/mL for 1 h at 4˚C before the addition of beads.

For m$^7$GTP pull down experiments, cells were lysed in cap lysis buffer (50 mM HEPES pH 7.4, 100 mM NaCl, 1 mM EDTA, 1% Nonidet P-40, protease inhibitor cocktail (Sigma P8340), and phosphatase inhibitor cocktail (Sigma P5762)), and incubated with 20 µL of pre-equilibrated γ-aminophenyl-m$^7$GTP beads (Jena Bioscience) at 4˚C overnight. The beads were washed three times with cap lysis buffer, and proteins were detected by immunoblotting as described above. Where indicated, the lysates were incubated with 100 µM m$^7$GpppG cap analogue at 4˚C for 30 min prior to the addition of γ-aminophenyl-m$^7$GTP beads.

**Protein purification and in vitro protein-protein interaction assays:** Hexahistidine-tagged IP6K1 was expressed in *Escherichia coli* BL21 (DE3) strain and purified using TALON metal affinity resin (Takara Bio) by standard procedures as described earlier (Azevedo et al., 2010). The recombinant GST fusion proteins were purified as described earlier (Chang et al., 2014) with minor modifications. Protein expression in *Escherichia coli* BL21 (DE3) strain was induced by overnight incubation with 0.4 mM IPTG at 20°C. Bacterial pellets were lysed by sonication in ice-cold lysis buffer (50 mM HEPES, pH 7.4, 200 mM NaCl, 5% glycerol, 2 mM DTT) supplemented with 10 µg/mL RNase A. The clarified lysate was mixed with 1% Triton X-100, and incubated with pre-equilibrated glutathione-agarose beads (GE Healthcare, 17-0756-01) at 4°C for 1 h. The resin was washed thrice with the lysis buffer containing 1% Triton X-100 to remove unbound proteins. For binding experiments, ~0.1 µM of each GST fusion protein immobilized on glutathione-agarose beads, was incubated with ~0.1 µM purified hexahistidine-tagged IP6K1 in ice-cold binding buffer (50 mM HEPES, pH 7.4, 200 mM NaCl, 5% glycerol, 2 mM DTT, 2 mM $MgCl_2$, 2 mM $MnCl_2$ and 1% Triton X-100) supplemented with protease inhibitor cocktail, at 4°C for 1 h. Following 5 washes with the binding buffer, proteins were eluted from beads in the presence of 1X Laemmli buffer, resolved by SDS-PAGE, and subjected to western blotting with anti-6xHis-tag antibody. GST-fusion proteins were visualized by Ponceau S staining of the PVDF membrane.

**RT-qPCR:** Total cellular RNA was isolated from U-2 OS shNT or sh*IP6K1* cells using TRIzol reagent (Invitrogen) for cell lysis, and RNeasy Mini Kit (Qiagen) for RNA extraction. Where indicated, U-2 OS cells were harvested for RNA isolation at indicated time points after treatment with 5 µg/mL Actinomycin D or DMSO. 2 µg RNA was used to synthesize cDNA by reverse transcription with oligonucleotide dT primers using SuperScript Reverse Transcriptase III (Invitrogen). Gene-specific primers were used to perform qPCR on the ABI 7500 Real-Time PCR System (Applied Biosystems) with MESA GREEN qPCR MasterMix Plus and SYBR® Assay Low ROX (Eurogentec) for detection. Each sample was run in technical duplicates. The sequences of primers used are listed in Table S1. The difference in transcript levels was calculated using the fold change ($\Delta\Delta C_t$) method (Schmittgen and Livak, 2008). $\Delta C_t$ is the $C_t$ value for the gene of interest normalized to the $C_t$ value of the respective GAPDH control in both U-2 OS shNT and U-2 OS sh*IP6K1* cells. For the data shown in Fig. S4A, $\Delta\Delta C_t$ values were calculated as a relative change in $\Delta C_t$ of the target gene in U-2 OS sh*IP6K1* cells with respect to U-2 OS shNT cells. For experiments shown in Fig. 6E and

S6C, $\Delta\Delta C_t$ values were calculated as a relative change in $\Delta C_t$ of the target gene in treated cells from each time point, with respect to untreated cells. Fold changes were expressed as $2^{-\Delta\Delta Ct}$. mRNA half-life was calculated by linear regression fit of ln(relative remaining mRNA) as a function of time, using the equation $t_{1/2} = \ln(2)/\text{slope}$.

**Subcellular fractionation of U-2 OS and HEK293T cells:** ~2 x$10^7$ cells were trypsinized, washed with 1X PBS, lysed by resuspension in Buffer C (50 mM Tris-Cl, pH 7.4, 250 mM sucrose, 250 mM KCl, 5 mM $MgCl_2$, and 0.7% Nonidet P-40), and centrifuged at 750 *g* to pellet the nuclear fraction. The post-nuclear supernatant was further centrifuged at 12,500 *g* to pellet the mitochondrial fraction. The concentration of KCl in the post-mitochondrial fraction (PMF) was adjusted to 0.5 M to disrupt weak interactions between proteins of other cellular compartments and the ribosomes. Finally, to obtain a ribosomal pellet, the PMF was layered on top of a sucrose cushion (1 M sucrose, 0.5 M KCl, 5 mM $MgCl_2$, and 50 mM Tris Cl, pH 7.4), and subjected to ultracentrifugation at 250,000 *g* at 4°C for 2 h. The ribosomes were present in a translucent and viscous pellet. The post-nuclear, ribosomal, and post-ribosomal fractions were boiled in 1X Laemmli buffer, and processed using standard western blotting techniques. For immunoprecipitation from ribosomes, the ribosomal pellet was resuspended in cell lysis buffer, and processed as described above.

**Luciferase based miRNA reporter assay:** The luciferase reporters used in this assay are described in (Pillai et al., 2005), and were obtained from Dr. Suvendra Bhattacharyya (CSIR-Indian Institute of Chemical Biology, Kolkata). HeLa shNT and HeLa sh*IP6K1* cells were transfected in a 24-well plate with 100 ng of pFL (firefly luciferase) transfection control plasmid, and 75 ng of pRL (Renilla luciferase) constructs (pRL control, pRL-perf, or pRL-3XB). 24 h post transfection, luciferase assay was performed using the Dual Luciferase Reporter Assay kit (Promega) as per the manufacturer's instructions. Luciferase activity was measured using the EnSpire Multimode Plate Reader (PerkinElmer). Renilla luciferase activity was normalized to firefly luciferase activity for each sample. These normalized values were expressed relative to the pRL control sample for each cell line.

**Polysome profiling:** Polysomes profiling in HeLa shNT and sh*IP6K1* cells expressing the luciferase reporter pRL-3XB was conducted as described earlier (Panda et al., 2017). Cells cultured to 70-80% confluence were incubated with 100 µg/mL cycloheximide (CHX) for 15

min, trypsinized, washed with ice-cold PBS containing 100 µg/mL CHX, and lysed in polysome lysis buffer (20 mM Tris Cl, pH 7.4, 100 mM KCl, 5 mM $MgCl_2$, 0.5% Nonidet P-40, 100 µg/mL CHX, 100 U RNase-OUT, and 1 mg/mL heparin, supplemented with protease inhibitor cocktail). Clarified lysate containing 175 µg RNA was loaded on top of a 10-50% sucrose gradient prepared in gradient buffer (20 mM Tris Cl, pH 7.4, 140 mM KCl, 5 mM $MgCl_2$, 100 µg/mL CHX, and 1 mg/mL heparin, supplemented with protease inhibitor cocktail), and centrifuged at 221,000 *g* for 3 h and 15 min at 4°C. After centrifugation, the gradients were analysed by measuring absorbance at 254 nm using a density gradient fractionator (Teledyne ISCO). The polysome-to-monosome ratios for each cell line were calculated using Fiji software.

**Decapping assay:** The mRNA decapping assay was performed as previously described (Tritschler et al., 2009). Briefly, a 176-bp luciferase cDNA fragment, amplified from pGL3-control plasmid (Promega), was transcribed and capped using the T7 mScript™ Standard mRNA Production System (CellScript). The RNA was labelled by adding 20 µCi of [α-$^{32}$P]GTP to the capping reaction. The RNA was purified after each step - transcription and capping – using the mirVana miRNA isolation kit (Invitrogen) total RNA isolation protocol. To obtain GFP-tagged DCP2 for the decapping assay, HEK293T cells transfected with plasmids encoding GFP-DCP2, or the GFP control, with or without myc-IP6K1 or myc-IP6K2, were lysed in NET-1 buffer (50 mM Tris-Cl pH 7.5, 150 mM NaCl, 1 mM EDTA, 0.1% Triton X-100, and 10% glycerol). GFP fusion proteins were immunoprecipitated as described above, with the exception that the last washing step was performed with NET-2 buffer (50 mM Tris-Cl, pH 7.5, 150 mM NaCl, 0.05% Triton X-100, and 0.1 mg/mL BSA, supplemented with protease and phosphatase inhibitor cocktail). Immunoprecipitates on Protein A Sepharose beads were resuspended in NET-2 buffer to form a 1:1 slurry. Half the immunoprecipitate was used for immunoblotting, and the remaining half was used for the decapping assay. The immunoprecipate was resuspended in decapping buffer (50 mM Tris-Cl, pH 7.9, 30 mM ammonium sulfate, and 1 mM $MgCl_2$), containing 0.1 mM cap structure analogue $m^7$GpppG (Jena Bioscience), 0.4 U/µL RNase inhibitor, and $10^5$ cpm of capped RNA, in a 15 µL reaction volume, and incubated for 30 min at 30°C with mixing at 900 rpm (Thermomixer R, Eppendorf). The reaction was stopped by the addition of 50 mM EDTA, 7 µL sample was spotted on a polyethylenimine (PEI) cellulose TLC plate (Sigma-Aldrich, Z122882), and resolved using 0.75 M LiCl. Unlabeled $m^7$GMP, $m^7$GDP, and $m^7$GTP were used as standards, and were visualized by UV shadowing. The radiolabelled capped mRNA

substrate and $m^7$GDP product were visualised by autoradiography (Typhoon FLA-9500, GE). The extent of decapping was measured by normalizing the intensity of the $m^7$GDP product to the intensity of total RNA.

**Statistical analysis.** GraphPad Prism 5 was used to perform statistical analyses and prepare graphs. Densitometry data for western blots were obtained using Fiji software (Schindelin et al., 2012). Band intensities of indicated proteins were normalized to their respective loading controls from the same blot. These normalized intensity values were expressed relative to the control in each blot, as detailed in the figure legends. The number of cells (n) used to perform statistical tests for each experiment, and the number of biologically independent replicates (N) for each experiment are indicated in the figure legends. *P* values are from either a one-sample *t*-test, a two-tailed unpaired Student's *t*-test, or a two-tailed Mann-Whitney test (for data that did not follow a normal distribution), as indicated in the respective figure legends. $P \leq 0.05$ was considered statistically significant.

**Acknowledgements**

The authors thank Suvendra Bhattacharyya for sharing Renilla luciferase miRNA reporters, and Maddika Subba Reddy for sharing the Gateway cloning vectors. We acknowledge H. H. Krishnan and Haripriya for their generous assistance with polysome profiling. We thank Aushaq Bashir Malla for initiating investigations into the effect of IP6K1 on P-bodies; Jayraj Sen for the generation of antibody directed against the N-terminus of IP6K1; Shubhra Ganguli for the generation of U-2 OS shNT and sh*IP6K1* cells, for the construction of SFB-IP6K1 K226A expression plasmid, and for assistance with the IP6 kinase assay; Sitalakshmi Thampatty for the construction of SFB-GFP and SFB-IP6K1 expression plasmid; Vineesha Oddi for the construction of IP6K1-V5 expression plasmid; and Aisha Hamid for the construction of IP6K1-V5 K226A expression plasmid. We thank Ravi Pal for assistance with the purification of recombinant GST fusion proteins. We acknowledge the staff at the Sophisticated Equipment Facility and Experimental Animal Facility, CDFD, for technical assistance. We thank Maddika Subba Reddy, Rohit Joshi, and members of the Laboratory of Cell Signalling for valuable feedback.

**Author contributions**

Conceived research: A.S. and R.B.; Designed and performed the experiments: A.S.; Data analysis: A.S. and R.B.; Wrote the paper: A.S. and R.B.

## Conflict of Interest

The authors declare that no conflict of interest exists.


## Funding

This work was supported by the Human Frontier Science Program (RGP0025/2016), Department of Biotechnology, Ministry of Science and Technology, Government of India (BT/PR29960/BRB/10/1762/2019), Science and Engineering Research Board, Department of Science and Technology, Government of India (CRG/2019/002597), and Centre for DNA Fingerprinting and Diagnostics core funds. A.S. is a recipient of Junior and Senior Research Fellowships from the University Grants Commission, Government of India.


## References


**Aizer A., Brody Y., Ler L.W., Sonenberg N., Singer R.H., and Shav-Tal Y.** (2008). The dynamics of mammalian P body transport, assembly, and disassembly in vivo. *Mol Biol Cell*, **19**, 4154-4166.

**Arribas-Layton M., Wu D., Lykke-Andersen J., and Song H.** (2013). Structural and functional control of the eukaryotic mRNA decapping machinery. *Biochim Biophys Acta*, **1829**, 580-589.

**Ayache J., Bénard M., Ernoult-Lange M., Minshall N., Standart N., Kress M., and Weil D.** (2015). P-body assembly requires DDX6 repression complexes rather than decay or Ataxin2/2L complexes. *Mol Biol Cell*, **26**, 2579-2595.

**Azevedo C., Burton A., Bennett M., Onnebo S.M., and Saiardi A.** (2010). Synthesis of InsP7 by the Inositol Hexakisphosphate Kinase 1 (IP6K1). *Methods Mol Biol*, **645**, 73-85.

**Bhandari R., Juluri K.R., Resnick A.C., and Snyder S.H.** (2008). Gene deletion of inositol hexakisphosphate kinase 1 reveals inositol pyrophosphate regulation of insulin secretion, growth, and spermiogenesis. *Proc Natl Acad Sci U S A*, **105**, 2349-2353.

**Chang C.T., Bercovich N., Loh B., Jonas S., and Izaurralde E.** (2014). The activation of the decapping enzyme DCP2 by DCP1 occurs on the EDC4 scaffold and involves a conserved loop in DCP1. *Nucleic Acids Res*, **42**, 5217-5233.

**Cougot N., Babajko S., and Seraphin B.** (2004). Cytoplasmic foci are sites of mRNA decay in human cells. *J Cell Biol*, **165**, 31-40.

**Erickson S.L., Corpuz E.O., Maloy J.P., Fillman C., Webb K., Bennett E.J., and Lykke-Andersen J.** (2015). Competition between decapping complex formation and ubiquitin-mediated proteasomal degradation controls human Dcp2 decapping activity. *Mol Cell Biol*, **35**, 2144-2153.

**Ferraiuolo M.A., Basak S., Dostie J., Murray E.L., Schoenberg D.R., and Sonenberg N.** (2005). A role for the eIF4E-binding protein 4E-T in P-body formation and mRNA decay. *J Cell Biol*, **170**, 913-924.

**Haas G., Braun J.E., Igreja C., Tritschler F., Nishihara T., and Izaurralde E.** (2010). HPat provides a link between deadenylation and decapping in metazoa. *J Cell Biol*, **189**, 289-302.

**Hubstenberger A., Courel M., Benard M., Souquere S., Ernoult-Lange M., Chouaib R., Yi Z., Morlot J.B., Munier A., Fradet M., Daunesse M., Bertrand E., Pierron G., Mozziconacci J., Kress M., and Weil D.** (2017). P-Body purification reveals the condensation of repressed mRNA regulons. *Mol Cell*, **68**, 144-157.e145.

**Jadav R.S., Chanduri M.V., Sengupta S., and Bhandari R.** (2013). Inositol pyrophosphate synthesis by inositol hexakisphosphate kinase 1 is required for homologous recombination repair. *J Biol Chem*, **288**, 3312-3321.

**Jadav R.S., Kumar D., Buwa N., Ganguli S., Thampatty S.R., Balasubramanian N., and Bhandari R.** (2016). Deletion of inositol hexakisphosphate kinase 1 (IP6K1) reduces cell migration and invasion, conferring protection from aerodigestive tract carcinoma in mice. *Cell Signal*, **28**, 1124-1136.

**Kamenska A., Simpson C., Vindry C., Broomhead H., Bénard M., Ernoult-Lange M., Lee B.P., Harries L.W., Weil D., and Standart N.** (2016). The DDX6-4E-T interaction mediates translational repression and P-body assembly. *Nucleic Acids Res*, **44**, 6318-6334.

**Kedersha N., Stoecklin G., Ayodele M., Yacono P., Lykke-Andersen J., Fritzler M.J., Scheuner D., Kaufman R.J., Golan D.E., and Anderson P.** (2005). Stress granules and processing bodies are dynamically linked sites of mRNP remodeling. *J Cell Biol*, **169**, 871-884.

**Kotaja N., Bhattacharyya S.N., Jaskiewicz L., Kimmins S., Parvinen M., Filipowicz W., and Sassone-Corsi P.** (2006). The chromatoid body of male germ cells: similarity with processing bodies and presence of Dicer and microRNA pathway components. *Proc Natl Acad Sci U S A*, **103**, 2647-2652.

**Liu J., Rivas F.V., Wohlschlegel J., Yates J.R., 3rd, Parker R., and Hannon G.J.** (2005). A role for the P-body component GW182 in microRNA function. *Nat Cell Biol*, **7**, 1261-1266.

**Lolla P., Shah A., C P.U., Oddi V., and Bhandari R.** (2021). Inositol pyrophosphates promote MYC polyubiquitination by FBW7 to regulate cell survival. *Biochem J*.

**Luo Y., Na Z., and Slavoff S.A.** (2018). P-Bodies: composition, properties, and functions. *Biochemistry*, **57**, 2424-2431.

**Luo Y., Schofield J.A., Simon M.D., and Slavoff S.A.** (2020). Global Profiling of Cellular Substrates of Human Dcp2. *Biochemistry*, **59**, 4176-4188.

**Malla A.B., and Bhandari R.** (2017). IP6K1 is essential for chromatoid body formation and temporal regulation of Tnp2 and Prm2 expression in mouse spermatids. *J Cell Sci*, **130**, 2854-2866.

**Maquat L.E., and Kiledjian M.** (2008). RNA turnover in eukaryotes: nucleases, pathways and analysis of mRNA decay. Preface. *Methods Enzymol*, **448**, xxi-xxii.

**Panda A.C., Martindale J.L., and Gorospe M.** (2017). Polysome Fractionation to Analyze mRNA Distribution Profiles. *Bio Protoc*, **7**.

**Parker R., and Sheth U.** (2007). P bodies and the control of mRNA translation and degradation. *Mol Cell*, **25**, 635-646.

**Pelechano V., Wei W., and Steinmetz L.M.** (2015). Widespread co-translational RNA decay reveals ribosome dynamics. *Cell*, **161**, 1400-1412.

**Pillai R.S., Bhattacharyya S.N., Artus C.G., Zoller T., Cougot N., Basyuk E., Bertrand E., and Filipowicz W.** (2005). Inhibition of translational initiation by Let-7 microRNA in human cells. *Science*, **309**, 1573-1576.

**Ramirez C.V., Vilela C., Berthelot K., and McCarthy J.E.** (2002). Modulation of eukaryotic mRNA stability via the cap-binding translation complex eIF4F. *J Mol Biol*, **318**, 951-962.

**Sahu S., Wang Z., Jiao X., Gu C., Jork N., Wittwer C., Li X., Hostachy S., Fiedler D., Wang H., Jessen H.J., Kiledjian M., and Shears S.B.** (2020). InsP(7) is a small-molecule regulator of NUDT3-mediated mRNA decapping and processing-body dynamics. *Proc Natl Acad Sci U S A*.

**Saiardi A., Erdjument-Bromage H., Snowman A.M., Tempst P., and Snyder S.H.** (1999). Synthesis of diphosphoinositol pentakisphosphate by a newly identified family of higher inositol polyphosphate kinases. *Curr Biol*, **9**, 1323-1326.

**Saiardi A., Nagata E., Luo H.R., Snowman A.M., and Snyder S.H.** (2001). Identification and characterization of a novel inositol hexakisphosphate kinase. *J Biol Chem*, **276**, 39179-39185.

**Schindelin J., Arganda-Carreras I., Frise E., Kaynig V., Longair M., Pietzsch T., Preibisch S., Rueden C., Saalfeld S., Schmid B., Tinevez J.-Y., White D.J., Hartenstein V., Eliceiri K., Tomancak P., and Cardona A.** (2012). Fiji: an open-source platform for biological-image analysis. *Nat Methods*, **9**, 676-682.

**Schmittgen T.D., and Livak K.J.** (2008). Analyzing real-time PCR data by the comparative CT method. *Nat Protocols*, **3**, 1101-1108.

**Schwartz D.C., and Parker R.** (2000). mRNA decapping in yeast requires dissociation of the cap binding protein, eukaryotic translation initiation factor 4E. *Mol Cell Biol*, **20**, 7933.

**Sheth U., and Parker R.** (2003). Decapping and decay of messenger RNA occur in cytoplasmic processing bodies. *Science*, **300**, 805-808.

**Standart N., and Weil D.** (2018). P-Bodies: Cytosolic droplets for coordinated mRNA storage. *Trends Genet*, **34**, 612-626.

**Sweet T., Kovalak C., and Coller J.** (2012). The DEAD-box protein Dhh1 promotes decapping by slowing ribosome movement. *PLoS Biol*, **10**, e1001342.

**Thomas M.P., and Potter B.V.** (2014). The enzymes of human diphosphoinositol polyphosphate metabolism. *FEBS J*, **281**, 14-33.

**Tritschler F., Braun J.E., Motz C., Igreja C., Haas G., Truffault V., Izaurralde E., and Weichenrieder O.** (2009). DCP1 forms asymmetric trimers to assemble into active mRNA decapping complexes in metazoa. *Proc Natl Acad Sci U S A*, **106**, 21591-21596.

**Vilela C., Velasco C., Ptushkina M., and McCarthy J.E.** (2000). The eukaryotic mRNA decapping protein Dcp1 interacts physically and functionally with the eIF4F translation initiation complex. *EMBO J*, **19**, 4372-4382.

**Wang H., DeRose E.F., London R.E., and Shears S.B.** (2014). IP6K structure and the molecular determinants of catalytic specificity in an inositol phosphate kinase family. *Nat Commun*, **5**, 4178.

**Wang Z., Jiao X., Carr-Schmid A., and Kiledjian M.** (2002). The hDcp2 protein is a mammalian mRNA decapping enzyme. *Proc Natl Acad Sci U S A*, **99**, 12663-12668.

**Weidner J., Wang C., Prescianotto-Baschong C., Estrada A.F., and Spang A.** (2014). The polysome-associated proteins Scp160 and Bfr1 prevent P body formation under normal growth conditions. *J Cell Sci*, **127**, 1992-2004.

**Yu J.H., Yang W.H., Gulick T., Bloch K.D., and Bloch D.B.** (2005). Ge-1 is a central component of the mammalian cytoplasmic mRNA processing body. *RNA*, **11**, 1795-1802.

**Zhang B., and Herman P.K.** (2020). It is all about the process(ing): P-body granules and the regulation of signal transduction. *Curr Genet*, **66**, 73-77.

**Zheng D., Ezzeddine N., Chen C.Y., Zhu W., He X., and Shyu A.B.** (2008). Deadenylation is prerequisite for P-body formation and mRNA decay in mammalian cells. *J Cell Biol*, **182**, 89-101.

**Figures**

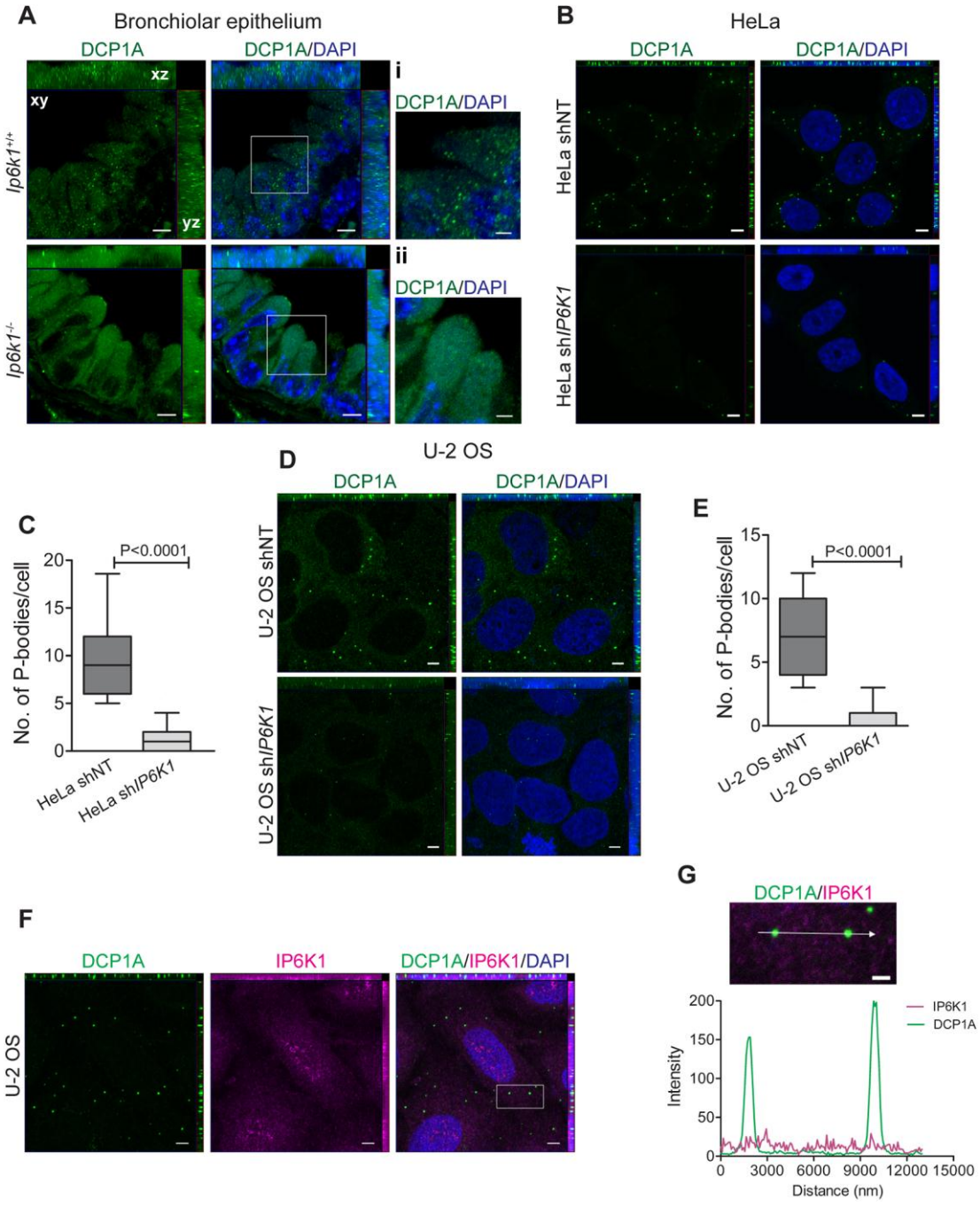


**Figure 1. Depletion of IP6K1 reduces the abundance of P-bodies. (A)** Representative bronchiolar epithelial cross sections from *Ip6k1*$^{+/+}$ and *Ip6k1*$^{-/-}$ mice were stained for P-body marker protein DCP1A (green). Nuclei were stained with DAPI (blue). Boxed areas in (A) were magnified, and are shown as insets (i) and (ii). Inset (i) shows granular P-body staining in *Ip6k1*$^{+/+}$ bronchiolar epithelial cells. Inset (ii) shows diffuse cytoplasmic staining in *Ip6k1*$^{-/-}$

bronchiolar epithelial cells. Scale bar in (A) is 5 μm and in insets (i) and (ii) is 2 μm, N=2. **(B)** Asynchronous HeLa shNT and sh*IP6K1* cells were stained with anti-DCP1A antibody (green). Nuclei were stained with DAPI (blue). Scale bar, 5 μm. **(C)** Box plot representation and quantification of the number of P-bodies/cell in (B). The box represents $25^{th}$ to $75^{th}$ percentile of the data set, with the centre line denoting the median value. Whiskers mark the $10^{th}$ and the $90^{th}$ percentile (n = 83 and 118 cells respectively, for HeLa shNT and sh*IP6K1* cells from three independent experiments) **(D)** Asynchronous U-2 OS shNT and sh*IP6K1* cells were stained with anti-DCP1A antibody (green). Nuclei were stained with DAPI (blue). Scale bar, 5 μm. **(E)** Box plot representation and quantification of the number of P-bodies/cell in (D). The box represents $25^{th}$ to $75^{th}$ percentile of the data set, with the centre line denoting the median value. Whiskers mark the $10^{th}$ and the $90^{th}$ percentile (n = 109 and 113 cells respectively, for U-2 OS shNT and sh*IP6K1* cells from three independent experiments). **(F)** Localization of IP6K1 (magenta) with DCP1A (green) in U-2 OS cells. Nuclei were stained with DAPI (blue). Scale bar, 5 μm, N=2. **(G)** The boxed region in (F) was magnified and fluorescence intensity profiles were measured along the line drawn. Scale bar, 2 μm. The green and magenta traces denote DCP1A and IP6K1 fluorescence intensities, respectively, and the two high intensity green peaks correspond to P-bodies. Images in (A), (B), (D) and (F) were subjected to uniform 'levels' adjustment in the ZEN software to improve visualization. *P* values in (C) and (E) are from a two-tailed Mann-Whitney test; $P \leq 0.05$ was considered significant. All confocal immunofluorescence images are z-stacks showing xy, yz and xz dimensions as a maximum intensity projection (see images marked in (A) as an example).

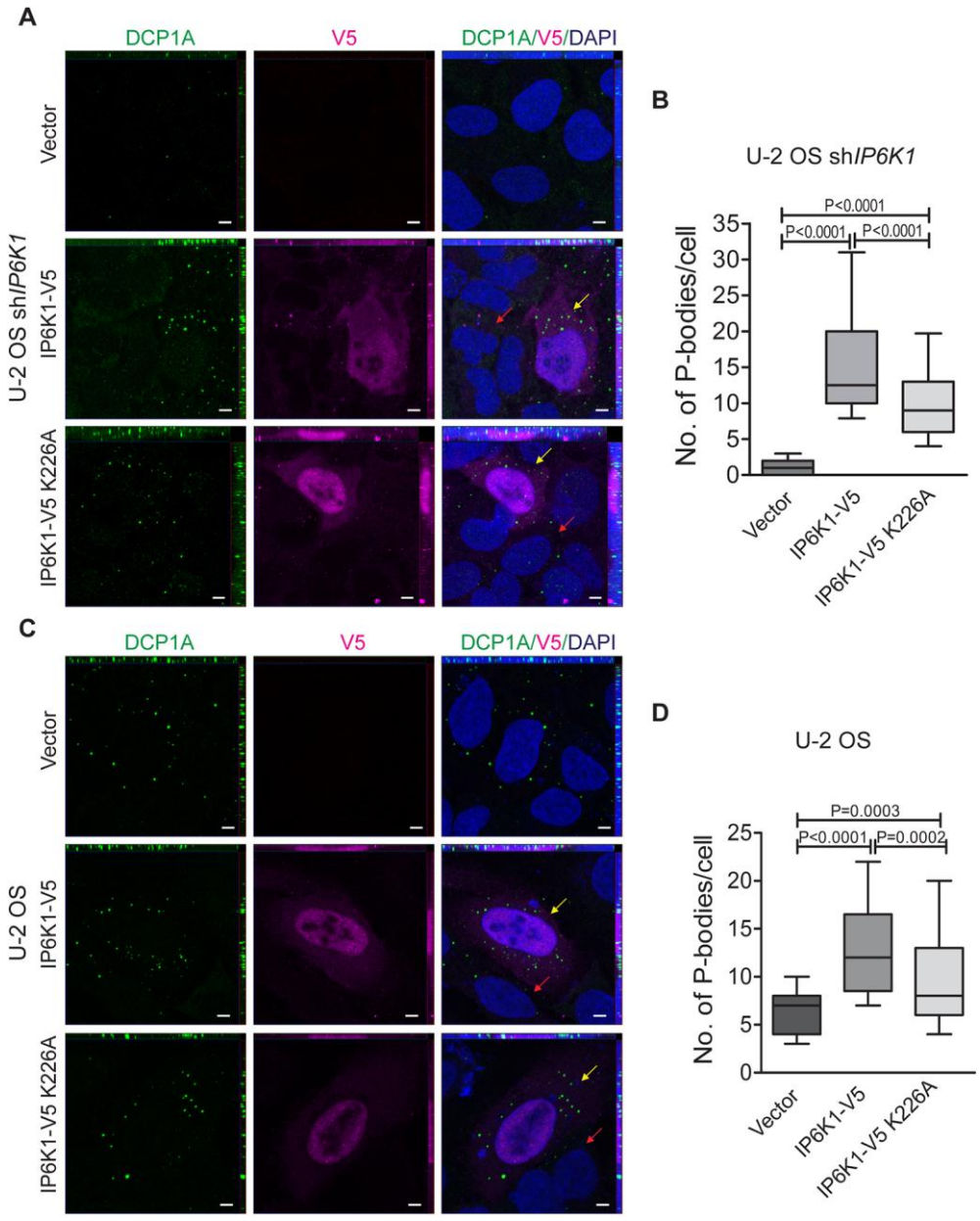


**Figure 2. P-body formation does not require IP6K1 catalytic activity. (A)** Asynchronous U-2 OS sh*IP6K1* cells overexpressing either V5-tagged IP6K1 (IP6K1-V5) or IP6K1-V5 K226A, or vector control (magenta) were stained with anti-DCP1A antibody (green). Nuclei were stained with DAPI (blue). Transfected and untransfected cells are indicated with yellow and red arrows, respectively. Scale bar, 5 μm. **(B)** Box plot representation and quantification of the number of P-bodies/cell in (A). The box represents 25$^{th}$ to 75$^{th}$ percentile of the data set, with the centre line denoting the median value. Whiskers mark the 10$^{th}$ and the 90$^{th}$ percentile (n = 110, 58, and 62 cells respectively, for U-2 OS sh*IP6K1* cells expressing vector, IP6K1-V5, or IP6K1-V5 K226A from two independent experiments). **(C)** Asynchronous U-2 OS cells overexpressing either IP6K1-V5 or IP6K1-V5 K226A, or vector

control (magenta) were stained with anti-DCP1A antibody (green). Nuclei were stained with DAPI (blue). Transfected and untransfected cells are indicated with yellow and red arrows, respectively. Scale bar, 5 μm. **(D)** Box plot representation and quantification of the number of P-bodies/cell in (C). The box represents $25^{th}$ to $75^{th}$ percentile of the data set, with the centre line denoting the median value. Whiskers mark the $10^{th}$ and the $90^{th}$ percentile (n = 72, 89, and 66 cells respectively, for U-2 OS cells expressing vector, IP6K1-V5, or IP6K1-V5 K226A, from three independent experiments). Images in (A) and (C) were subjected to uniform 'levels' adjustment in the ZEN software to improve visualization. *P* values are from a two-tailed Mann-Whitney test (B and D); $P \leq 0.05$ was considered significant. All confocal immunofluorescence images are z-stacks showing xy, yz and xz dimensions as a maximum intensity projection.

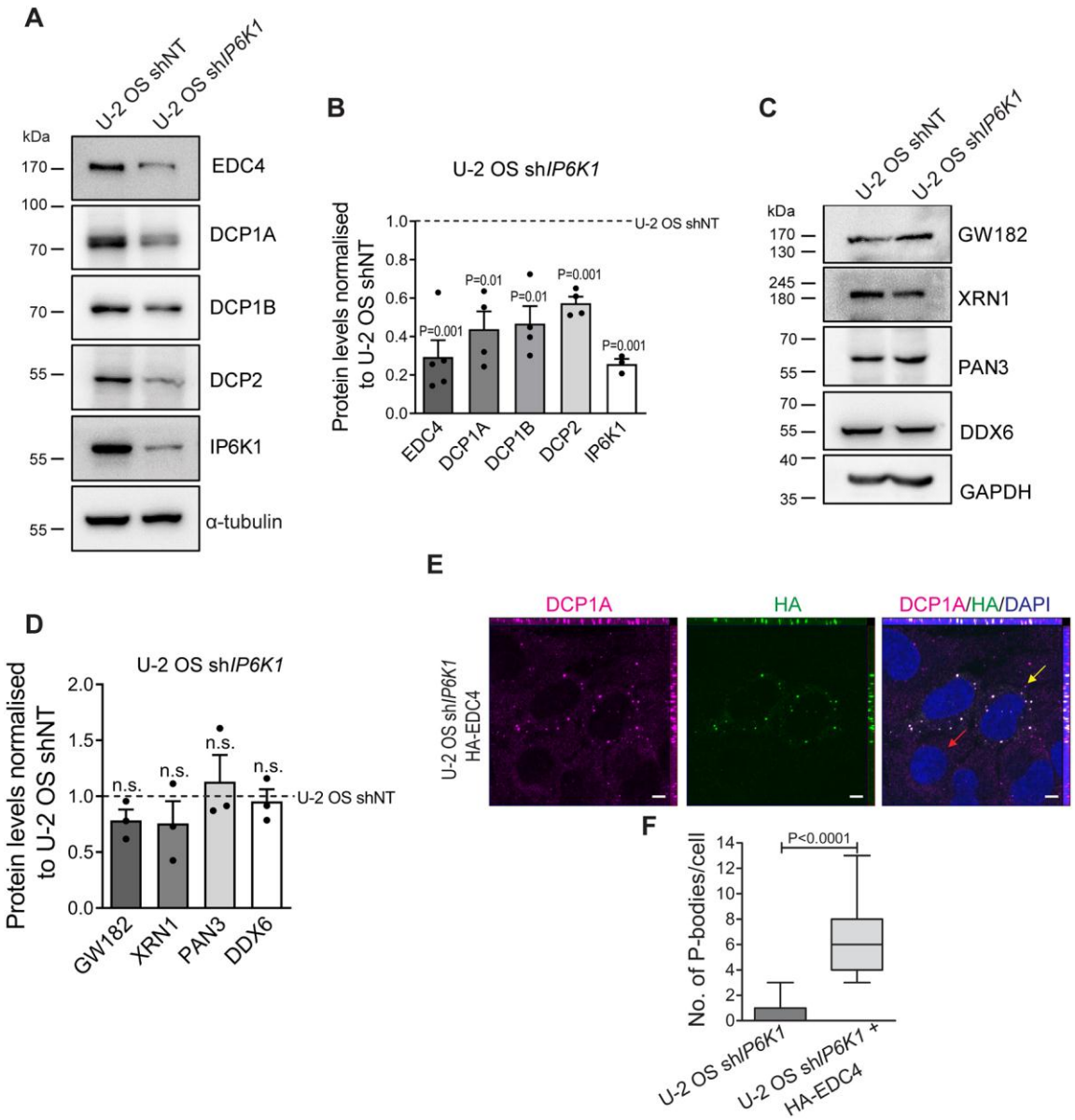


**Figure 3. Reduced IP6K1 levels leads to downregulation of mRNA decapping proteins.** **(A)** Representative immunoblots showing steady state levels of mRNA decapping proteins in U-2 OS shNT and sh*IP6K1* cells. Tubulin was used as a loading control. **(B)** Data show mean fold change ± s.e.m. in the protein levels from (A) in U-2 OS sh*IP6K1* cells over U-2 OS shNT cells, N=3 for IP6K1, N=4 for DCP1A, DCP1B, and DCP2 and N=5 for EDC4. **(C)** Representative immunoblots showing steady state levels of proteins that function up- or down-stream to mRNA decapping in U-2 OS shNT and sh*IP6K1* cells. GAPDH was used as a loading control. **(D)** Data show mean fold change ± s.e.m. in the protein levels from (C) in U-2 OS sh*IP6K1* cells over U-2 OS shNT cells, N=3. **(E)** Asynchronous U-2 OS sh*IP6K1* cells overexpressing HA epitope-tagged EDC4 (magenta) were stained with anti-DCP1A antibody (green). Nuclei were stained with DAPI (blue). Transfected and untransfected cells

are indicated with yellow and red arrows, respectively. Scale bar, 5 μm. **(F)** Box plot representation and quantification of the number of P-bodies/cell in (E). The box represents $25^{th}$ to $75^{th}$ percentile of the data set, with the centre line denoting the median value. Whiskers mark the $10^{th}$ and the $90^{th}$ percentile (n = 56 and 58 cells, respectively, for untransfected and HA-EDC4-transfected cells from two independent experiments). Images in (E) were subjected to uniform 'levels' adjustment in the ZEN software to improve visualization. *P* values are from a one sample *t*-test (B and D), or a two-tailed Mann-Whitney test (F); $P \leq 0.05$ was considered significant; n.s., not significant $P > 0.05$. All confocal immunofluorescence images are z-stacks showing xy, yz and xz dimensions as a maximum intensity projection.

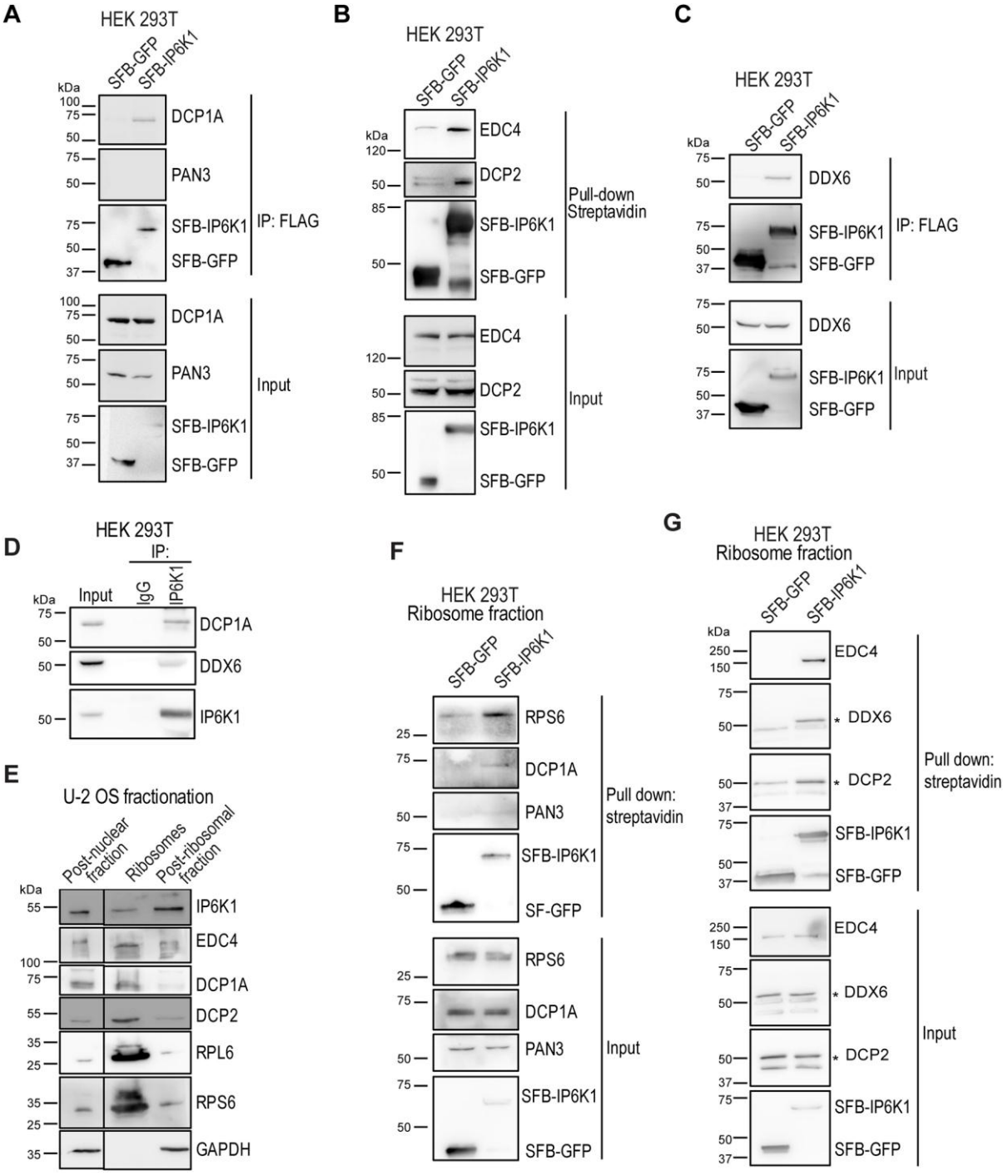


**Figure 4. IP6K1 interacts with the mRNA decapping complex on ribosomes. (A-C)** Representative immunoblots examining co-immunoprecipitation of endogenous DCP1A, PAN3, EDC4, DCP2, and DDX6 with SFB-tagged IP6K1. SFB-IP6K1 or SFB-GFP were transiently overexpressed in HEK293T cells, pulled-down with either anti-FLAG antibody (A and C), or streptavidin sepharose beads (B), and probed to detect DCP1A, PAN3, EDC4, DCP2, or DDX6. The SFB tag was detected using an anti-FLAG antibody (N=3). There was some weak interaction of EDC4 and DCP2 with SFB-GFP, albeit lower than the binding of

these proteins to SFB-IP6K1. **(D)** Representative immunoblots examining co-immunoprecipitation of endogenous DCP1A and DDX6 with endogenous IP6K1. A HEK293T cell extract was subjected to immunoprecipitation with an antibody directed against the N-terminal region of IP6K1, and probed to detect DCP1A or DDX6 (N=3). **(E)** Representative immunoblots of subcellular fractions of U-2 OS cells, to detect endogenous IP6K1, EDC4, DCP1A, and DCP2. Enrichment of ribosomes was marked by the presence of RPL6 and RPS6, and GAPDH was detected to rule out cytoplasmic contamination in the ribosomal fraction (N=4). Vertical line indicates removal of non-essential lanes from a single original gel to improve visualisation. **(F and G)** Representative immunoblots examining co-immunoprecipitation of endogenous RPS6, DCP1A, PAN3, EDC4, DDX6 and DCP2 with SFB-tagged IP6K1 in ribosomes. The ribosomal fraction isolated from HEK293T cells transiently overexpressing SFB-IP6K1 or SFB-GFP was subjected to pull-down with streptavidin sepharose beads, and probed to detect the indicated proteins (N=3 for RPS6 and EDC4, and N=4 for DCP1A, DCP2 and DDX6). There was some weak interaction of DCP2 with SFB-GFP, albeit lower than its binding to SFB-IP6K1. The asterisk (*) in (G) indicates specific bands.

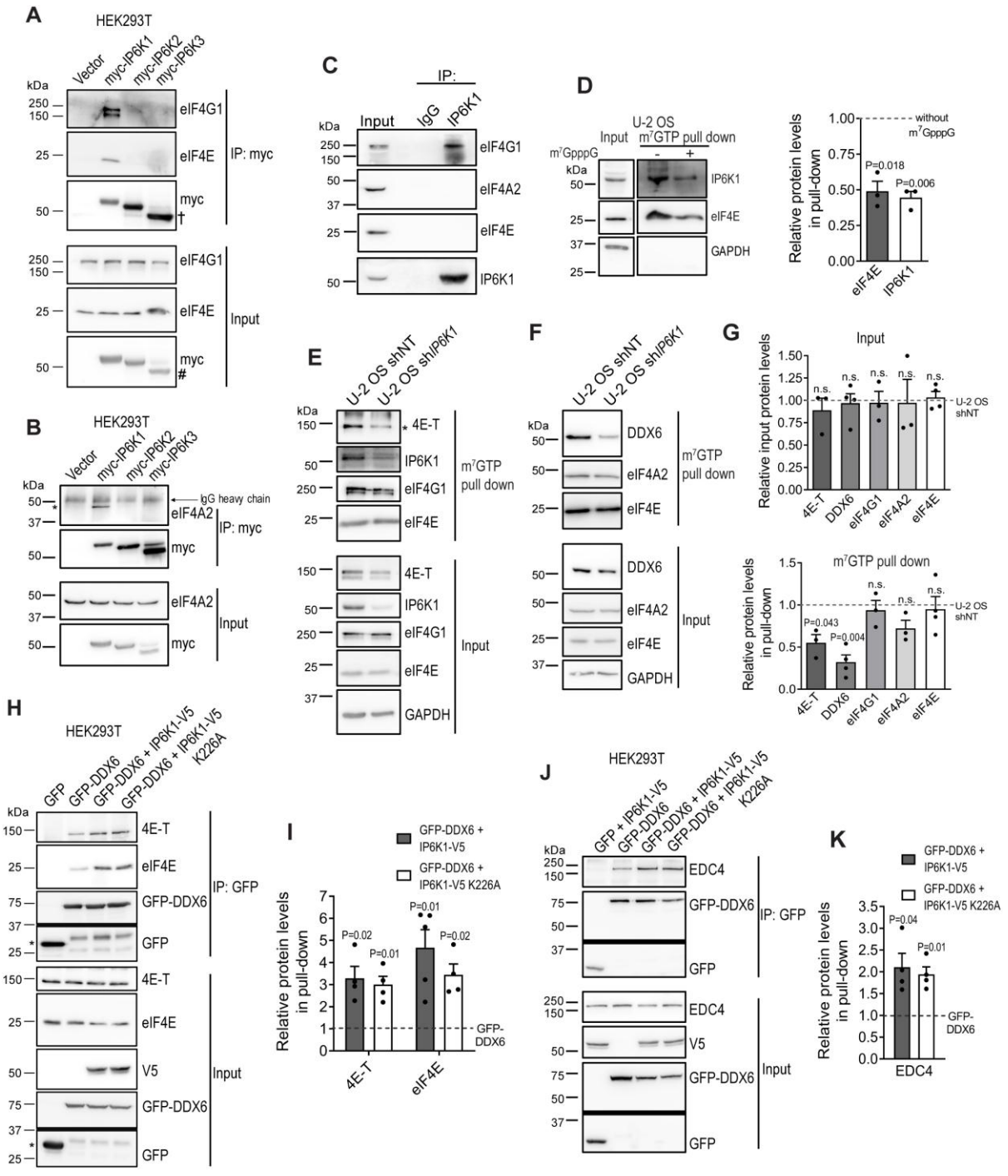


**Figure 5. IP6K1 binds the translation initiation complex eIF4F at the mRNA cap. (A and B)** Representative immunoblots examining co-immunoprecipitation of endogenous eIF4F complex with myc-tagged IP6Ks. Myc-IP6K1, myc-IP6K2 or myc-IP6K3 were transiently overexpressed in HEK293T cells, immunoprecipitated with an anti-myc antibody, and probed to detect eIF4E, eIF4G1, or eIF4A2. The myc-tagged IP6Ks were detected using an anti-myc antibody (N=2). The dagger (†) and hash (#) symbols indicate that the myc-tag immunoblots in (A) are identical to the myc-tag immunoblots presented in Fig. S5C, as the

blots in these panels are from a single original gel. **(C)** Representative immunoblots examining co-immunoprecipitation of endogenous eIF4G1, eIF4A2, or eIF4E with endogenous IP6K1. A HEK293T cell extract was subjected to immunoprecipitation with an antibody directed against the N-terminal region of IP6K1, and probed to detect eIF4G1, eIF4A2, or eIF4E (N=3). **(D)** A U-2 OS cell extract was incubated with $m^7$GTP–sepharose beads in the presence or absence of the cap analogue $m^7$GpppG, and subjected to immunoblotting to detect IP6K1 and eIF4E. Bar graphs show mean fold change ± s.e.m. in the extent of pull-down of IP6K1 and eIF4E in the presence of cap analogue when compared with the absence of cap analogue (N=3). **(E-G)** Representative immunoblots of proteins pulled down from U-2 OS shNT and sh*IP6K1* cell extracts by $m^7$GTP–sepharose beads. Bar graphs show mean fold change ± SEM in the expression levels (upper) and the extent of pull-down (lower) of the indicated proteins from U-2 OS sh*IP6K1* cells compared with U-2 OS shNT cells (N=3 for 4E-T, eIF4G1 and eIF4A2, and N=4 for DDX6 and eIF4E). **(H-K)** Representative immunoblots showing the effect of overexpression of V5 epitope-tagged IP6K1 or IP6K1 K226A on the extent of pull-down of endogenous 4E-T and eIF4E (H, I), or EDC4 (J, K) with GFP-tagged DDX6, from HEK293T cell extracts. Bar graphs show the mean fold change ± s.e.m. in the extent of co-immunoprecipitation when either IP6K1 or IP6K1 K226A was co-overexpressed with GFP-DDX6, compared with GFP-DDX6 overexpression alone (N=4). Horizontal lines between immunoblots indicate division of a single membrane into two parts that were immunoblotted separately, but were subjected to identical exposure during image acquisition. An asterisk (*) indicates specific bands in (B), (E) and (H). *P* values are from a one sample *t*-test (D, G, I and K); $P \leq 0.05$ was considered significant; n.s., not significant $P > 0.05$.

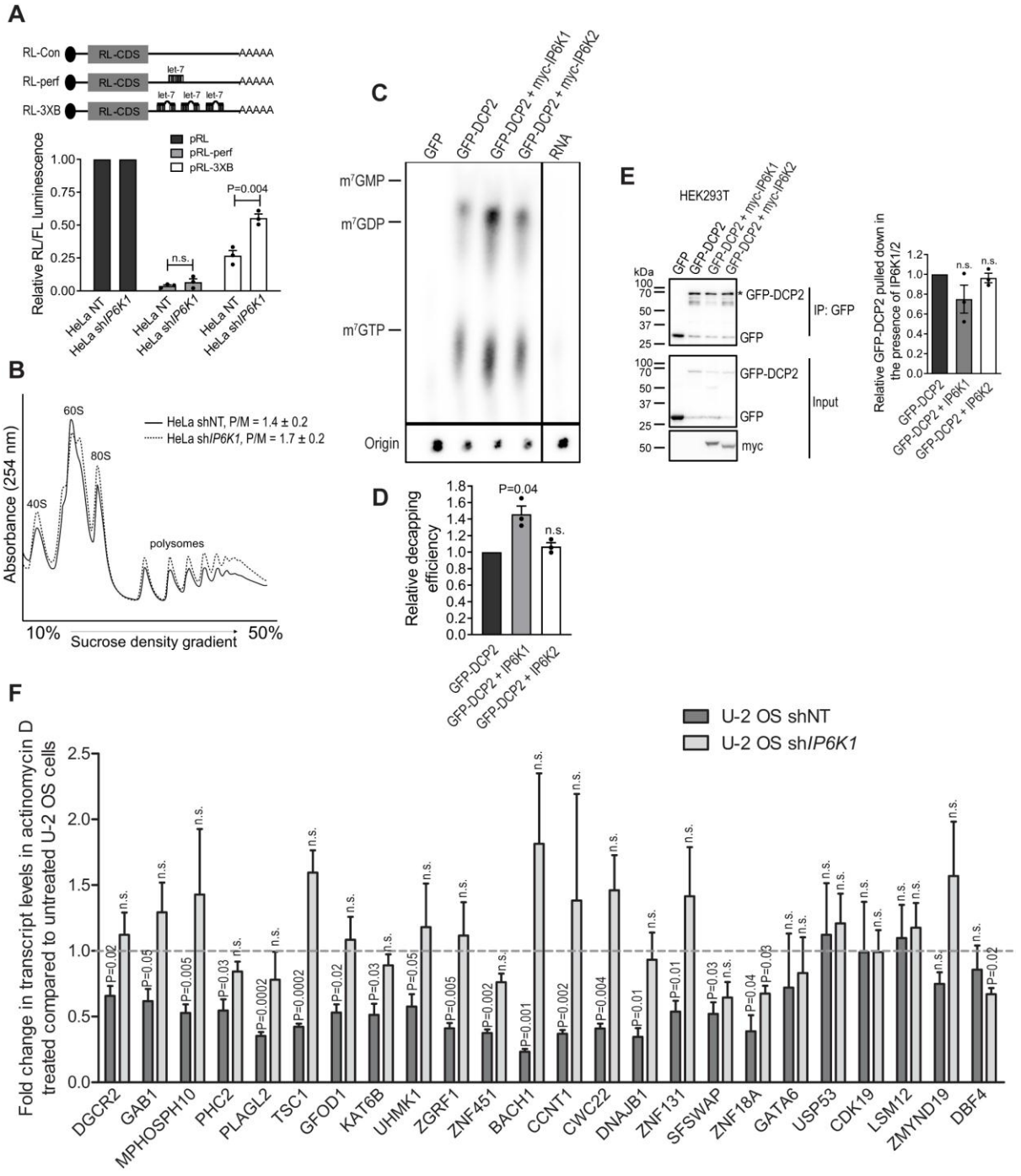


**Figure 6. IP6K1 promotes translational suppression and mRNA decapping**. **(A)** HeLa shNT and sh*IP6K1* cells were transfected with Renilla luciferase (RL) reporter constructs - pRL-control (no let-7a binding site in the 3'UTR), pRL-perf (perfect complimentary let7a binding site in the 3'UTR), or pRL-3xB (3 imperfect let-7a binding sites in the 3'UTR). Firefly luciferase (FL) was co-transfected to serve as an internal control. Relative RL/FL luminescence ratio was calculated, and normalised to the pRL control for each cell line. Data are mean ± s.e.m., N=3. *P* values are from a two-tailed unpaired Student's *t*-test; $P \leq 0.05$

was considered significant; n.s., not significant $P > 0.05$. **(B)** Polysome profiles of HeLa shNT and sh*IP6K1* cells expressing pRL-3xB, as measured by absorbance at 254 nm. The positions of 40S and 60S ribosomal subunits, 80S monosomes, and polysomes are indicated. The polysome-to-monosome ratios for each cell line are presented as mean ± s.e.m, N=3. **(C)** Representative autoradiogram showing the effect of IP6K1 and IP6K2 on DCP2-mediated mRNA decapping**.** Either GFP or GFP-tagged DCP2 were transiently overexpressed in HEK293T cells, with or without myc-IP6K1 or myc-IP6K2. Proteins were immunoprecipitated with an anti-GFP antibody, and half of the immunoprecipitate was incubated with $^{32}$P cap-labelled mRNA. The reaction mix was resolved by thin layer chromatography, and the mRNA substrate and hydrolyzed $m^7$GDP cap were visualized by autoradiography. Non-radioactive standards were run in parallel and visualized by UV shadowing. The vertical line indicates removal of non-essential lanes from a single original chromatogram for better depiction, and the horizontal line indicates the two parts that were subjected to differential auto-contrast adjustment for better visualization of the $m^7$GDP product. **(D)** Quantification of (C). The extent of decapping by DCP2 in the presence of myc-IP6K1 or myc-IP6K2, was quantified and normalized to the extent of decapping by DCP2 alone. Data (mean ± s.e.m., N=3), were analysed using a one-sample *t*-test. $P \leq 0.05$ was considered significant, n.s., not significant $P > 0.05$. **(E)** Half of the immunoprecipitate from (C) was subjected to immunoblotting with anti-GFP and anti-myc antibodies (left). The extent of immunoprecipitation of GFP-DCP2 when it was co-expressed with either IP6K1 or IP6K2, was normalized to GFP-DCP2 co-expression with the vector control (right). Data (mean fold change ± s.e.m., N=3) were analysed using a one-sample *t*-test. n.s., not significant $P > 0.05$. **(F)** RT-qPCR analysis of DCP2 substrate transcripts in U-2 OS shNT and sh*IP6K1* cells before and after treatment with Actinomycin D (5 µg/mL for 2 h). Values indicate the fold change in transcript levels in Actinomycin D treated cells over untreated cells. Data (mean ± s.e.m., N=3 or 4), were analysed using a one-sample *t*-test. $P \leq 0.05$ was considered significant, n.s., not significant $P > 0.05$.

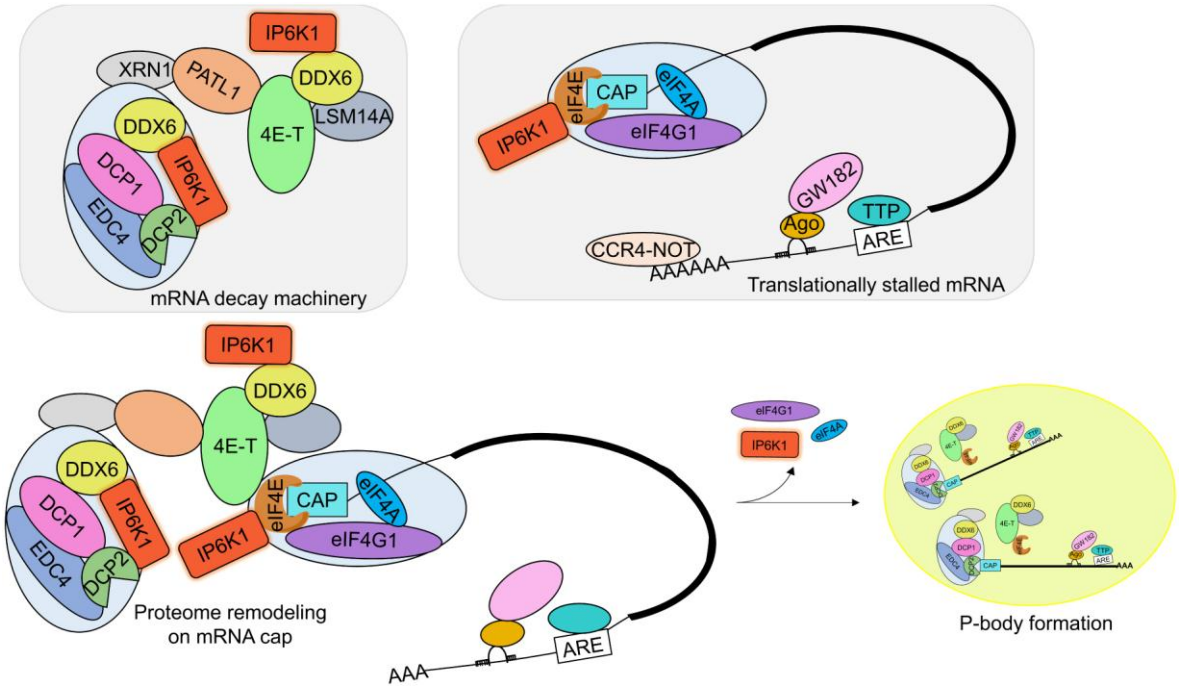


**Figure 7. IP6K1 facilitates proteome remodelling on the mRNA cap to promote translational suppression.** IP6K1 associates with the mRNA decapping complex *via* DCP2 and DDX6, and with the translation initiation complex *via* eIF4E. Other proteins that constitute the mRNA decapping complex and the translation initiation complex (shown inside light blue capsules) interact either directly or indirectly with IP6K1. The ability of IP6K1 to exhibit multi-protein interactions allows it to promote assembly of proteins that facilitate translational suppression. Specifically, IP6K1 upregulates interaction between members of the translation suppression complex 4-ET and DDX6, and enhances binding of this complex with the cap binding protein eIF4E. IP6K1 also increases binding of the decapping enhancer EDC4 to DDX6. These enhanced interactions subsequently lead to P-body formation.

Figure S1

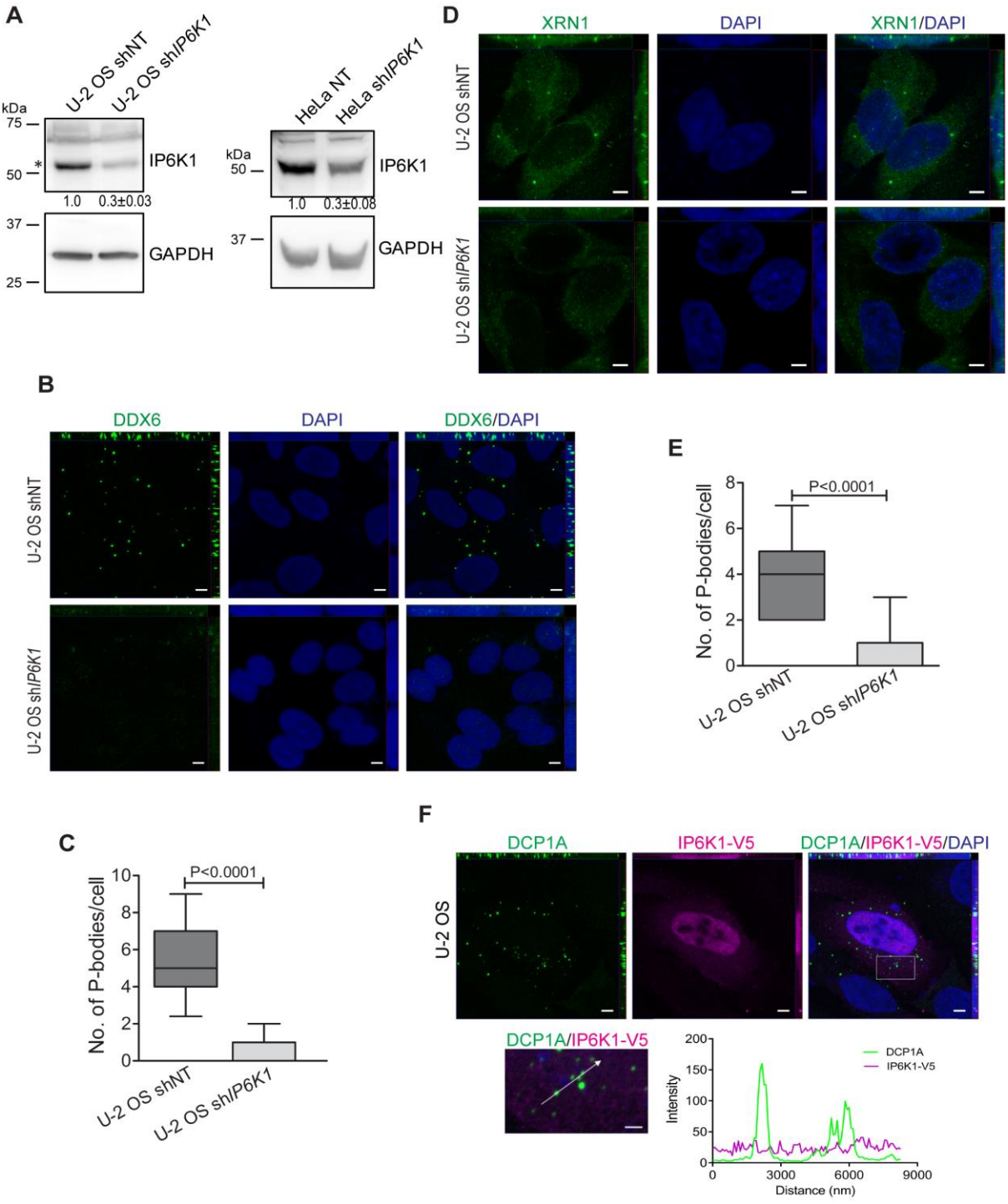


**Fig. S1. Overexpressed IP6K1 does not localize to P-bodies. (A)** Representative immunoblots to detect IP6K1 in U-2 OS (left) and HeLa (right) cells stably expressing either non-targeting control shRNA (shNT), or two different shRNA directed against human IP6K1 (sh*IP6K1*). GAPDH was used as a loading control. Numbers show mean fold change ± s.e.m.;

N=4 for U-2 OS and N=3 for HeLa cells. The extent of IP6K1 knockdown in U-2 OS cells is also shown as a bar graph in Fig. 3B. **(B)** Asynchronous U-2 OS shNT and sh*IP6K1* cells were stained with anti-DDX6 antibody (green). Nuclei were stained with DAPI (blue). Scale bar, 5 µm. **(C)** Box plot representation and quantification of the number of P-bodies/cell in (B). The box represents $25^{th}$ to $75^{th}$ percentile of the data set, with the centre line denoting the median value. Whiskers mark the $10^{th}$ and the $90^{th}$ percentile (n = 91 and 119 cells respectively, for U-2 OS shNT and sh*IP6K1* cells from two independent experiments). **(D)** Asynchronous U-2 OS shNT and sh*IP6K1* cells were stained with anti-XRN1 antibody (green). Nuclei were stained with DAPI (blue). Scale bar, 5 µm. **(E)** Box plot representation and quantification of the number of P-bodies/cell in (D). The box represents $25^{th}$ to $75^{th}$ percentile of the data set, with the centre line denoting the median value. Whiskers mark the $10^{th}$ and the $90^{th}$ percentile (n = 51 and 71 cells respectively, for U-2 OS shNT and sh*IP6K1* cells from two independent experiments). **(F)** Localization of V5 epitope-tagged IP6K1 (magenta) with DCP1A (green) in U-2 OS cells. Nuclei were stained with DAPI (blue). Scale bar, 5 µm, N=3. The boxed region in (F) is magnified and shown below, where intensity profiles were measured along the line drawn. Scale bar, 2 µm. The green and magenta traces denote DCP1A and IP6K1 fluorescence intensities, respectively, and the high intensity green peaks correspond to P-bodies. *P* values are from a two-tailed Mann-Whitney test (C and E); $P \leq 0.05$ was considered significant. Images in (B), (D), and (F) were subjected to uniform 'levels' adjustment in the ZEN software to improve visualization. All confocal immunofluorescence images are z-stacks showing xy, yz and xz dimensions as a maximum intensity projection.

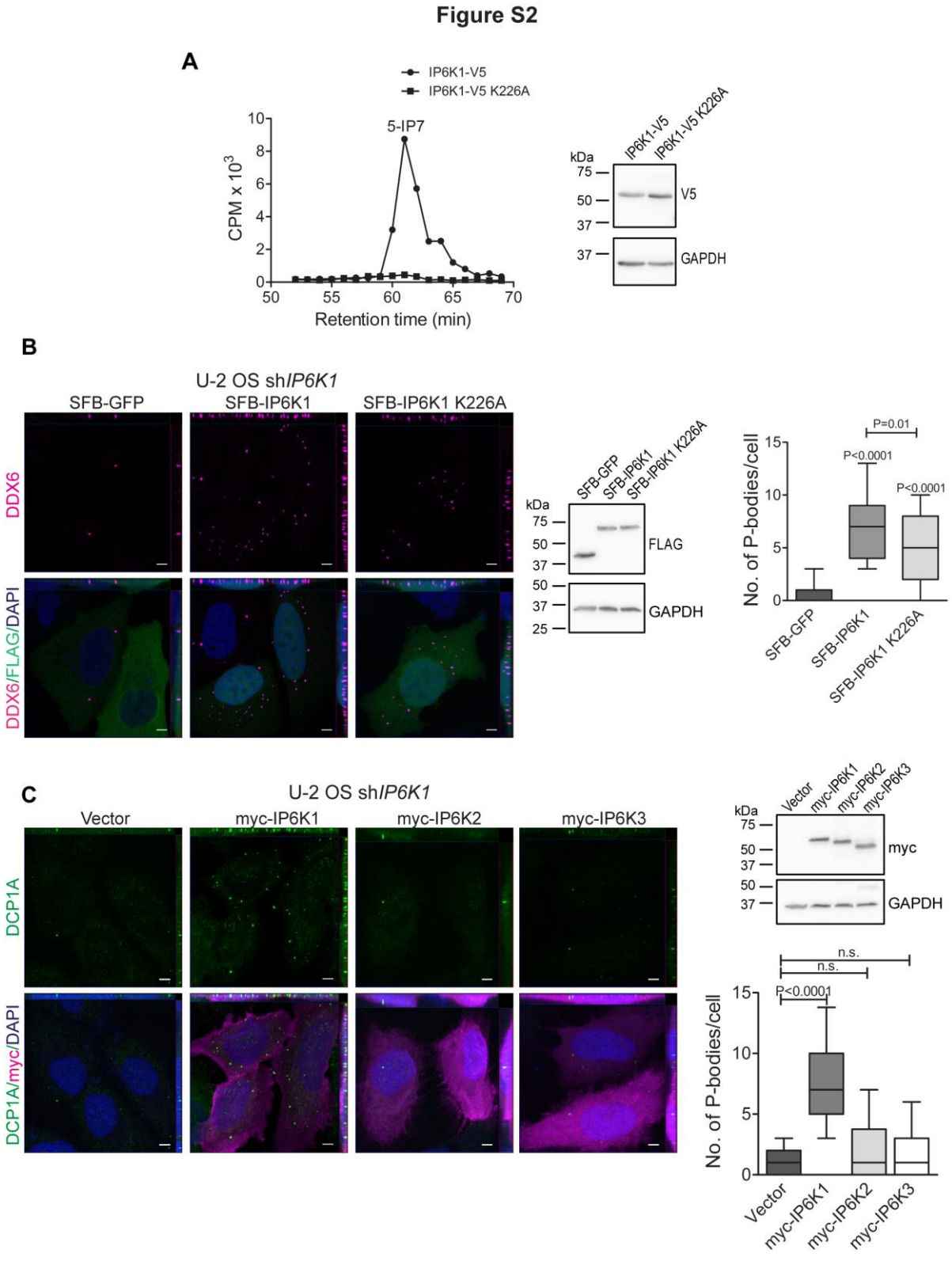


**Fig. S2. IP6K2 or IP6K3 do not rescue the loss of P-bodies in IP6K1-depleted cells. (A)** HPLC profile of [5β-$^{32}$P]-IP$_7$ formed during the incubation of immunoprecipitated IP6K1-V5 or IP6K1-V5 K226A with [γ-$^{32}$P]ATP and IP$_6$. The levels of IP6K1-V5 and IP6K1-V5 K226A overexpressed in HEK293T cells are shown to the right of HPLC profile. **(B)** Asynchronous

U-2 OS sh*IP6K1* cells overexpressing either SFB-IP6K1, SFB-IP6K1 K226A, or SFB-GFP control (magenta) were stained with anti-DDX6 antibody (green) (left). Nuclei were stained with DAPI (blue). Scale bar, 5 µm. Representative immunoblot to detect SFB-GFP, SFB-IP6K1, or SFB-IP6K1 K226A overexpressed in U-2 OS sh*IP6K1* cells (centre). Cofilin was used as a loading control. Box plot representation and quantification of the number of P-bodies/cell (right). The box represents 25$^{th}$ to 75$^{th}$ percentile of the data set, with the centre line denoting the median value. Whiskers mark the 10$^{th}$ and the 90$^{th}$ percentile (n = 57, 72, and 79 cells respectively, for U-2 OS sh*IP6K1* cells expressing SFB-GFP, SFB-IP6K1, and SFB-IP6K1 K226A overexpressing cells from two independent experiments). **(C)** Asynchronous U-2 OS sh*IP6K1* cells overexpressing either myc-IP6K1, myc-IP6K2, myc-IP6K3, or vector control (magenta) were stained with anti-DCP1A antibody (green) (left). Nuclei were stained with DAPI (blue). Scale bar, 5 µm. Representative immunoblot to detect myc-tagged IP6K1, IP6K2, or IP6K3, overexpressed in U-2 OS sh*IP6K1* cells (upper right). GAPDH was used as a loading control. Box plot representation and quantification of the number of P-bodies/cell (lower right). The box represents 25$^{th}$ to 75$^{th}$ percentile of the data set, with the centre line denoting the median value. Whiskers mark the 10$^{th}$ and the 90$^{th}$ percentile (n = 62, 51, 96, and 101 cells respectively, for U-2 OS sh*IP6K1* cells expressing vector, myc-IP6K1, myc-IP6K2, or myc-IP6K3, from two independent experiments). Images in (B) and (C) were subjected to uniform 'levels' adjustment in the ZEN software to improve visualization. All confocal immunofluorescence images are z-stacks showing xy, yz and xz dimensions as a maximum intensity projection.

## Figure S3

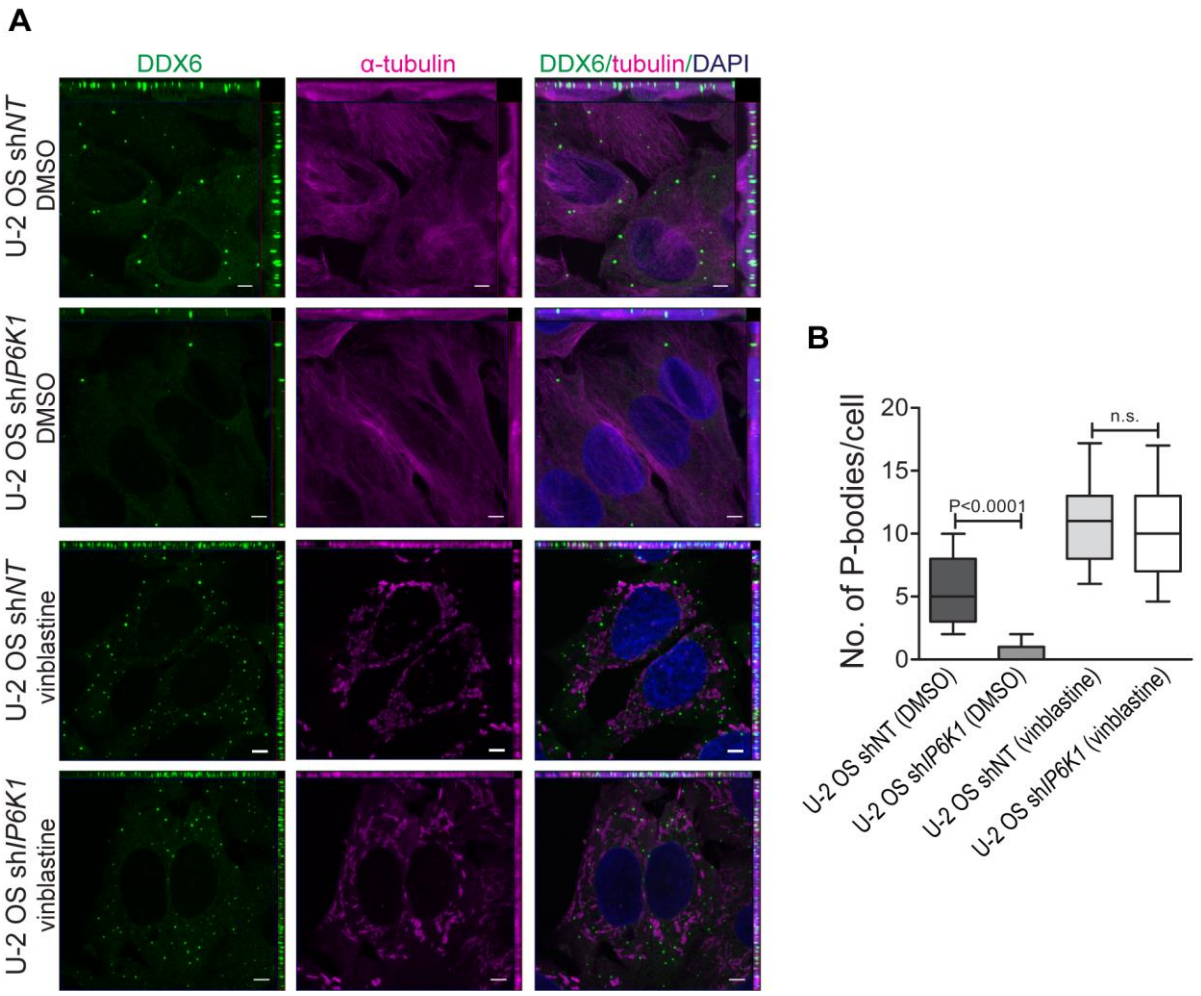


**Fig. S3. IP6K1 is not required for P-bodies induced upon treatment with vinblastine.** **(A)** Asynchronous U-2 OS shNT and sh*IP6K1* cells were treated with vinblastine (10 µM for 1 h) or DMSO as the vehicle control, and stained with anti-DDX6 antibody (green) and anti-α tubulin antibody (magenta). Nuclei were stained with DAPI (blue). Scale bar, 5 µm. **(B)** Box plot representation and quantification of the number of P-bodies/cell in (A). The box represents 25$^{th}$ to 75$^{th}$ percentile of the data set, with the centre line denoting the median value. Whiskers mark the 10$^{th}$ and the 90$^{th}$ percentile (n = 59, 83, 97, and 115 cells respectively, for U-2 OS shNT vehicle treated, U-2 OS sh*IP6K1* vehicle treated, U-2 OS shNT vinblastine treated, and U-2 OS sh*IP6K1* vinblastine treated cells from two independent experiments). *P* values are from a two-tailed Mann-Whitney test (B and E); $P \leq 0.05$ was considered significant, n.s., not significant $P > 0.05$. Images in (A) were subjected to uniform 'levels' adjustment in the ZEN software to improve visualization. All confocal immunofluorescence images are z-stacks showing xy, yz and xz dimensions as a maximum intensity projection.

**Figure S4**

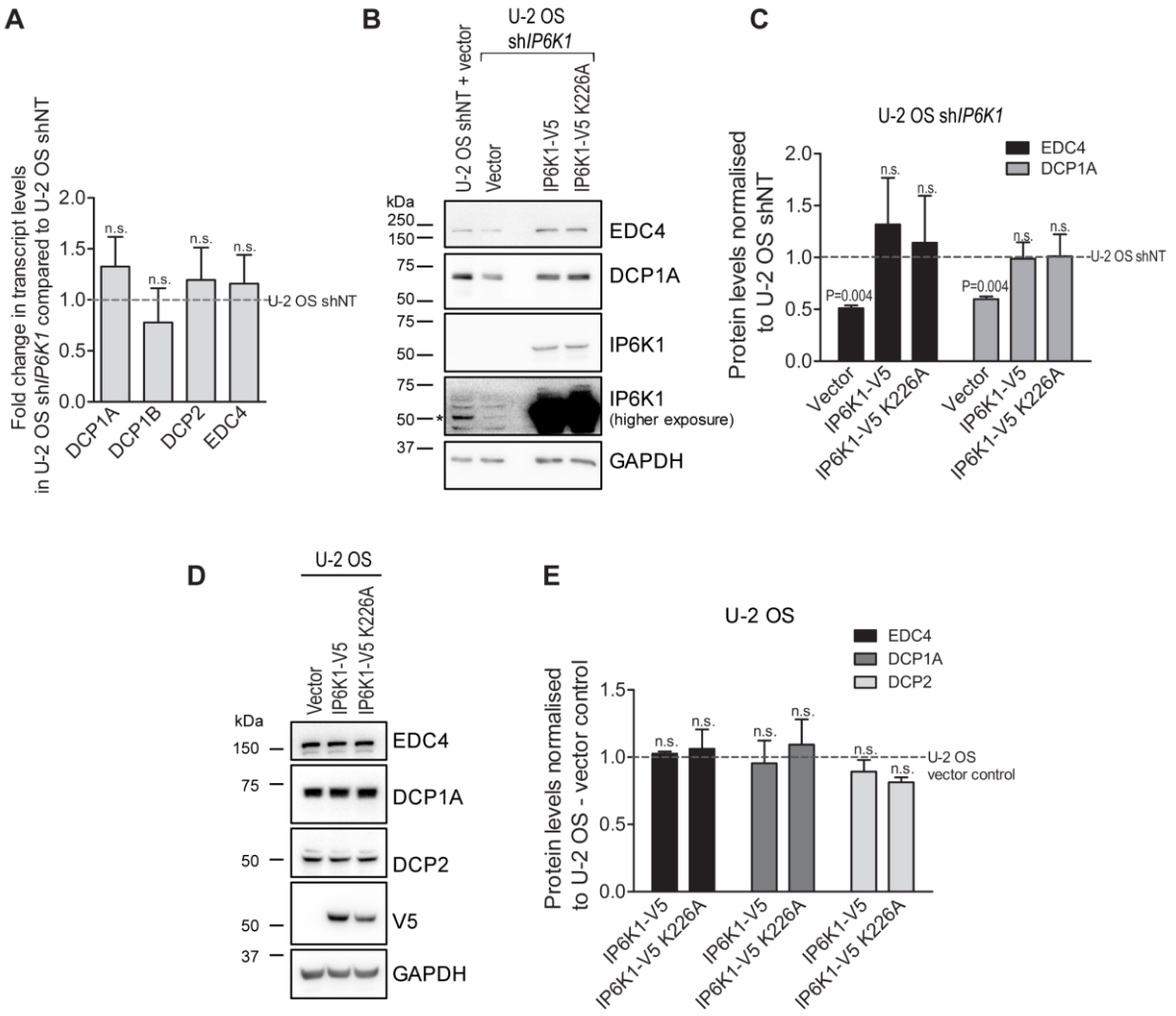


**Fig. S4. IP6K1 overexpression does not upregulate level of mRNA decapping proteins.** **(A)** RT-qPCR analysis of transcripts encoding mRNA decapping proteins that were observed to be downregulated in Fig. 3A. Values indicate the fold change in transcript levels in U-2 OS sh*IP6K1* cells normalized to U-2 OS shNT cells. Data are mean ± s.e.m., N=3 for DCP1B, and N=4 for DCP1A, DCP2, and EDC4. **(B)** Representative immunoblots showing the levels of mRNA decapping proteins in U-2 OS shNT cells transfected with vector control, and U-2 OS sh*IP6K1* cells overexpressing either IP6K1 or IP6K1 K226A, or vector control. GAPDH was used as a loading control. **(C)** Protein levels from (B) were normalized to their respective loading control. Data show mean fold change ± s.e.m. in the protein levels from (B) in U-2 OS sh*IP6K1* cells compared with U-2 OS shNT cells, N=3. **(D)** Representative immunoblots showing the levels of mRNA decapping proteins in U-2 OS cells overexpressing either IP6K1 or IP6K1 K226A, or vector control. GAPDH was used as a loading control. **(E)** Protein levels

from (D) were normalized to their respective loading control. Data show mean fold change ± s.e.m. in the protein levels from (D) in U-2 OS cells overexpressing either IP6K1 or IP6K1 K226A compared with U-2 OS cells transfected with vector control, N=3. *P* values are from a one sample *t*-test (C and E); $P \leq 0.05$ was considered significant; n.s., not significant $P > 0.05$.

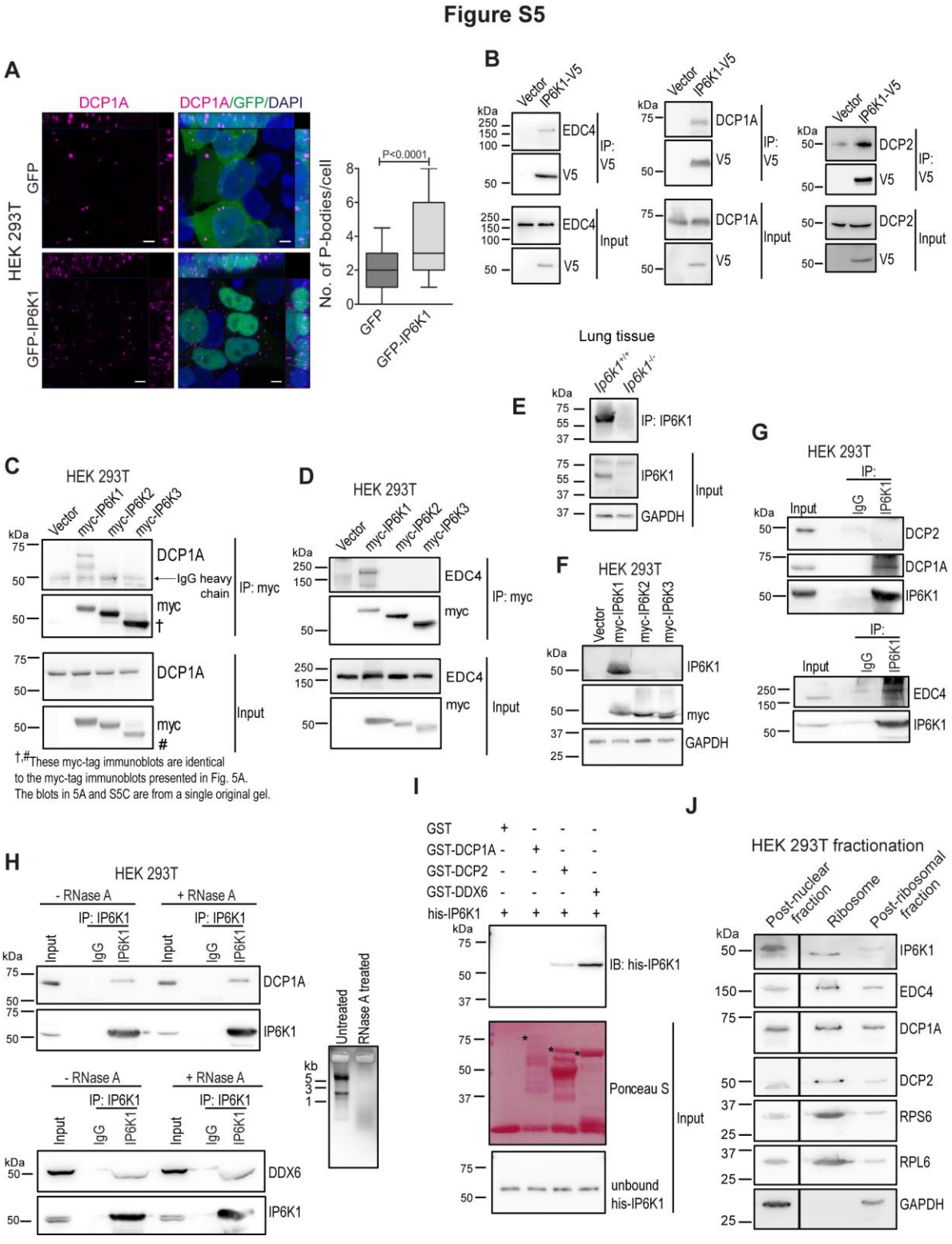


**Fig. S5. Interaction of IP6K1 with mRNA decapping proteins is RNA independent.**

**(A)** Asynchronous HEK 293T cells overexpressing either GFP-IP6K1 or GFP vector control (green) were stained with anti-DCP1A antibody (magenta) (left). Nuclei were stained with

DAPI (blue). Scale bar, 5 μm. Images were subjected to uniform 'levels' adjustment in the ZEN software to improve visualization. All confocal immunofluorescence images are z-stacks showing xy, yz and xz dimensions as a maximum intensity projection. Box plot representation and quantification of the number of P-bodies per GFP or GFP-IP6K1 expressing cell (right). The box represents 25$^{th}$ to 75$^{th}$ percentile of the data set, with the centre line denoting the median value. Whiskers mark the 10$^{th}$ and the 90$^{th}$ percentile (n = 64 and 73 cells respectively, for GFP and GFP-IP6K1 overexpressing cells from two independent experiments). *P* values are from a two-tailed Mann-Whitney test; $P \leq 0.05$ was considered significant. **(B)** Representative immunoblots examining co-immunoprecipitation of endogenous EDC4, DCP1A, and DCP2 with V5-tagged IP6K1. IP6K1-V5 or vector control were transiently expressed in HEK293T cells, immunoprecipitated with anti V5 antibody, and probed to detect EDC4, DCP1A, or DCP2 (N=3 for EDC4 and DCP1A, and N=2 for DCP2). There was some weak interaction of DCP2 with vector control, albeit lower than the binding of these proteins to IP6K1-V5. **(C and D)** Representative immunoblots examining co-immunoprecipitation of endogenous DCP1A and EDC4 with myc-tagged IP6K1, IP6K2 or IP6K3. Myc-IP6K1, myc-IP6K2, or myc-IP6K3 were transiently overexpressed in HEK 293T cells, immunoprecipitated with an anti-myc antibody, and probed to detect DCP1A or EDC4. Myc-IP6Ks were detected using an anti-myc antibody (N=2). The decapping proteins specifically interact with myc-IP6K1, but not with myc-IP6K2 or myc-IP6K3. The dagger (†) and hash (#) symbols indicate that the myc-tag immunoblots in (C) are identical to the myc-tag immunoblots presented in Fig. 5A, as the blots in these panels are from a single original gel. **(E and F)** Immunoblots to demonstrate the specificity of the antibody raised against the N-terminus of mouse IP6K1 (amino acid residues 1-22), generated in our laboratory. This sequence is identical in human and mouse protein. Homogenates of *Ip6k1*$^{+/+}$ and *Ip6k1*$^{-/-}$ mouse lung tissue were subjected to immunoprecipitation by the N-terminus IP6K1 antibody, followed by detection using a commercially available IP6K1 antibody (Sigma-Aldrich, HPA040825). GAPDH was used as a loading control (E). Myc-IP6K1, myc-IP6K2, or myc-IP6K3 were transiently overexpressed in HEK 293T cells, and probed with either N-terminus IP6K1 antibody or myc-tag antibody (F). **(G)** Representative immunoblots examining co-immunoprecipitation of endogenous DCP2, DCP1A, or EDC4 with endogenous IP6K1. A HEK293T cell extract was subjected to immunoprecipitation with an antibody directed against the N-terminal region of IP6K1, and probed to detect DCP2, DCP1A, or EDC4 (N=3). **(H)** Representative immunoblots showing co-immunoprecipitation of endogenous DCP1A and DDX6 with endogenous IP6K1 from untreated and RNase A-treated cell extracts (left). IP6K1 was immunoprecipitated with the N-

terminus IP6K1 antibody, and probed to detect DCP1A and DDX6 (N=3 for DCP1A, and N=2 for DDX6). A denaturing agarose gel showing ethidium bromide stained RNA extracted from HEK293T cells and subjected to incubation with or without RNase A (100 µg/mL for 30 min at $4^0$C; right). **(I)** Representative immunoblots examining direct binding of immobilized GST, GST-DCP1A, GST-DCP2, and GST-DDX6 with purified hexahistidine-tagged IP6K1 (6xHis-IP6K1). Interaction of 6xHis-IP6K1 with GST-tagged proteins was detected by immunoblotting with an anti-6xHis antibody. GST-tagged proteins were visualized by staining with Ponceau S. Unbound 6xHis-IP6K1 from the post-interaction supernatant was detected by immunoblotting with an anti-6xHis antibody (N=4 for GST-DCP2 and GST-DDX6; N=3 for GST-DCP1A). The asterisk (*) indicates specific bands corresponding to GST fusion proteins. **(J)** Representative immunoblots of subcellular fractions of HEK 293T cells prepared by ultracentrifugation, to detect endogenous IP6K1, EDC4, DCP1A, and DCP2. Enrichment of ribosomes was marked by the presence of RPL6 and RPS6, and GAPDH was detected to rule out cytoplasmic contamination in the purified ribosomes (N=2). Vertical line indicates removal of non-essential lanes from a single original gel to improve visualisation.

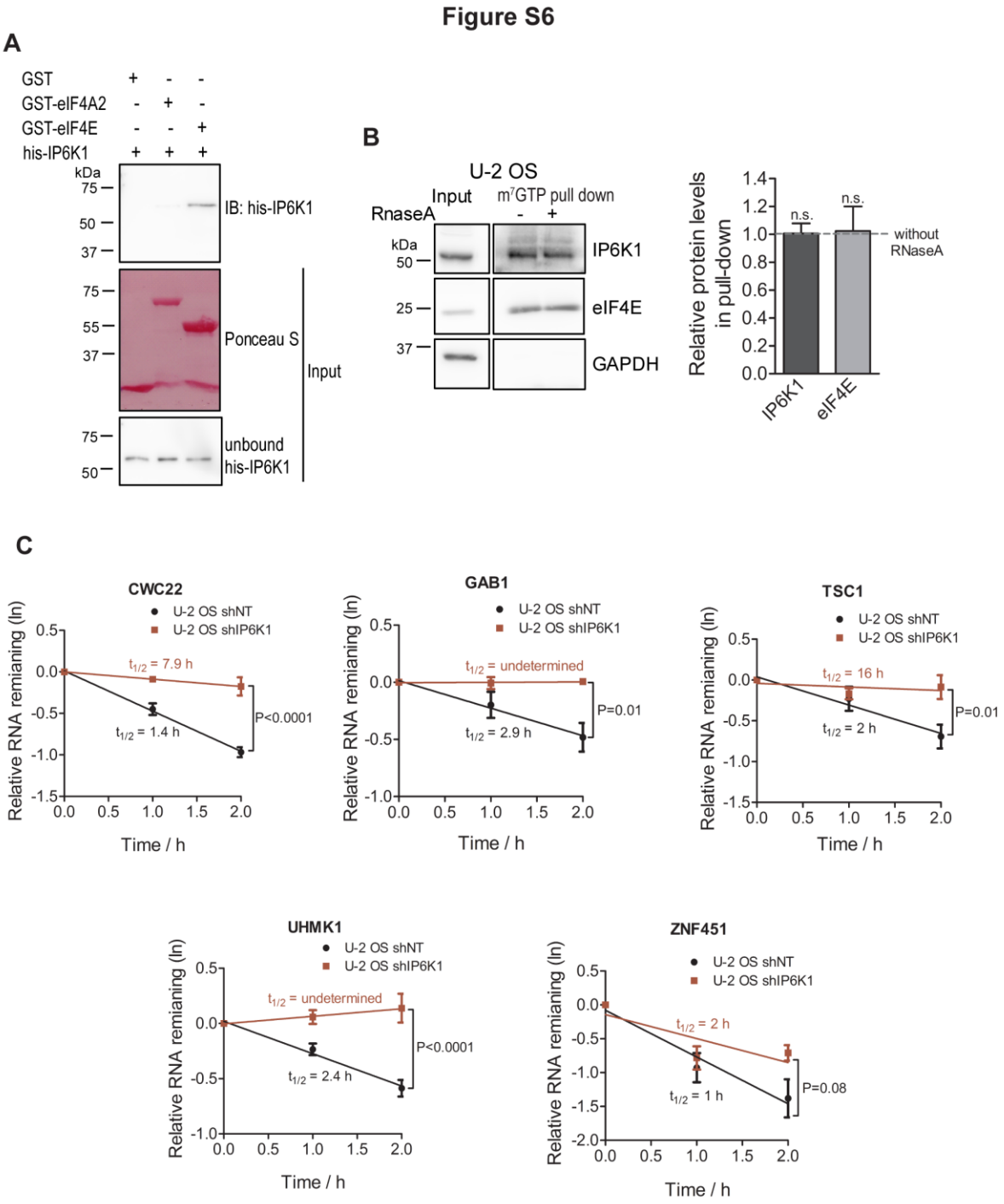


**Fig. S6. Interaction of IP6K1 with eIF4E (A)** Representative immunoblots demonstrating direct binding of immobilized GST, GST-eIF4A2, or GST-eIF4E with purified 6xHis-IP6K1. Interaction of 6xHis-IP6K1 with GST-tagged proteins was detected by immunoblotting with an anti-his antibody. GST-tagged proteins were visualized by staining with Ponceau S. Unbound 6xHis-IP6K1 from the post-interaction supernatant was detected by immunoblotting with an anti-6xHis antibody (N=3). **(B)** A U-2 OS cell extract was incubated with $m^7$GTP–

sepharose beads in the presence or absence of RNase A, and subjected to immunoblotting to detect IP6K1 and eIF4E. Bar graphs show mean fold change ± s.e.m. in the extent of pull-down of IP6K1 and eIF4E in the presence compared with the absence of RNase A (N=3). *P* values are from a one sample *t*-test; n.s., not significant $P > 0.05$. **(C)** The levels of selected DCP2 target mRNAs were measured using qRT-PCR in U-2 OS shNT and U-2 OS sh*IP6K1* cells following treatment with actinomycin D for the indicated time. The data was plotted as natural log of mRNA level relative to untreated cells in each experiment as a function of time. Half-lives were obtained from linear regression analysis; *P* values are from a two-tailed *t*-test of the slope of regression lines. $P \leq 0.05$ was considered significant. Error bars show mean ± s.e.m., N=4.

**Table S1.** Primers used for RT-qPCR analysis shown in Fig. S4A and 6E

| **Transcript** | **Primer** |
|---|---|
| *DCP1A* | F: 5'- AATAAAGAATGATTCCAGCTTCCTC -3'<br>R: 5'- AGCCTATTTGTCTCTGAGGCTG -3' |
| *DCP1B* | F: 5'- TATGTCTGGGAGGGAGGGAAG -3'<br>R: 5'- CACATCAGTTTTCTCCCACTCGT -3' |
| *DCP2* | F: 5'- TGGAAGGTTGTTCAGATACTGGC -3'<br>R: 5'- AGAGCAACCACAATGAGCAAC -3' |
| *EDC4* | F: 5'- ATTACAAGGGCCGATGCAGG -3'<br>R: 5'- GCTGCTGCAAGTATTCCTGTG -3' |
| *GFOD1* | F: 5'- GACTGACCACATCAAGGGCAT -3'<br>R: 5'- CGGGCACGTTGAAGTTGAG -3' |
| *CCNT1* | F: 5'- CGTGTCCCTCATTCGAAACT -3'<br>R: 5'- GAGCAGGGAGTGAAGCATATT -3' |
| *GATA6* | F: 5'- GAGCGCTGTTTGTTTAGGGC -3'<br>R: 5'- TACTGCTCTGCCGGAAAACT -3' |
| *GAB1* | F: 5'- GAGCCTTTGGCCCTCTAATA -3'<br>R: 5'- CTTACTTGACAGTGGAGGAGAAG -3' |
| *DGCR2* | F: 5'- AGGATCCCTGGCTTTGATTAC -3'<br>R: 5'- CGATGTCCGGGTACTTGTATG -3' |
| *PHC2* | F: 5'- AGGGAACGGAAACTCTGCCT -3'<br>R: 5'- TCGATAACATGCGTCAGGATTTG -3' |
| *KAT6B* | F: 5'- GAGCCTACCTGTGAGATTGAAG -3'<br>R: 5'- CCTTCCTCTTCCTCTGTTTGTC -3' |
| *DNAJB1* | F: 5'- AAGGCATGGACATTGATGACC -3'<br>R: 5'- GGCCAAAGTTCACGTTGGT -3' |
| *BACH1* | F: 5'- CCGCTTCAGTCTCTACCATATC -3'<br>R: 5'- GCCACTGTATTCTGAGTCCTATT -3' |
| *ZGRF1* | F: 5'- AGACCTGACTCCTACGGAAA -3'<br>R: 5'- GCACAGGTAACTCCAACTACTC -3' |
| *LSM12* | F: 5'- CCAGACCATTCACAAGACCATT -3'<br>R: 5'- TTGGCTTTCCACGTCTCTAAAAT -3' |

| | |
|---|---|
| *TSC1* | F: 5'- GCAGTGGGTAGTTCTAAGGATG -3'<br>R: 5'- GACTCTGCCCTTAACGCTTAT -3' |
| *ZNF18A* | F: 5'- CGGGAAGTTAGGGCTAAAGAAA -3'<br>R: 5'- CATAAGGCTGGTGGAAGAAGAG -3' |
| *DBF4* | F: 5'- GGGCAAAAGAGTTGGTAGTGG -3'<br>R: 5'- ACTTATCGCCATCTGTTTGGATT -3' |
| *ZNF451* | F: 5'- GGAGGAGCAGCAGTATGTAATC -3'<br>R: 5'- GCCACACTGGGTTTCTGTAA -3' |
| *SFSWAP* | F: 5'- CCACCGAGAGAAGAAGAGAAAG -3'<br>R: 5'- GATAGGCACTGGGAAGAGAATG -3' |
| *UHMK1* | F: 5'- GCATTGTGCCCGAGATGTTTT -3'<br>R: 5'- ATGTTACGTGGTTTGAGGTCC -3' |
| *ZNF131* | F: 5'- TGCCAACAGTAGCCTCATAAA -3'<br>R: 5'- TGCTTTCCATACATCATTGGCTT -3' |
| *CDK19* | F: 5'- TGCCAACAGTAGCCTCATAAA -3'<br>R: 5'- GCTTGCTCCGAGGTAATTCT -3' |
| *ZMYND19* | F: 5'- ACCGACTTCAAATTGGGTATCG -3'<br>R: 5'- CACTTCCATTCGGGCCTCAA -3' |
| *CWC22* | F: 5'- GGAAAAGGTCTCGGAAATCCC -3'<br>R: 5'- CCACCAGTGCGAGTAAGAAGA -3' |
| *MPHOSPH10* | F: 5'- AAATTGGATGCCCTCTCAAACTT -3'<br>R: 5'- CTCGTTTCTTGTCTGTAGCTGT -3' |
| *PLAGL2* | F: 5'- ACCATAGCTAGCCAGTCATTTC -3'<br>R: 5'- GGGTACTGAGTGCAGGATAAAG -3' |
| *USP53* | F: 5'- CATAGTGCCAAGCAGAGATGC -3'<br>R: 5'- CTCCACAGCTACGACACACA -3' |